GRAVITY SURVEY OF MOINONIN AREA IN LAKE BARINGO GEOTHERMAL PROSPECT, KENYA

CHARLES CHIRCHIR CHEMOSONG [BSC]

I56/CE/22364/2010

A research thesis submitted in partial fulfillment of the requirements for the award of the degree of Master of Science in the school of Pure and Applied Sciences of Kenyatta University

September, 2018

DECLARATION

I Charles Chirchir Chemosong declare that this thesis is my original work and has not been presented for the award of a degree or any other award in any other university or any other award.

Signature..... Date.....

Charles Chirchir Chemosong
Department of Physics
Kenyatta University

SUPERVISORS

We confirm that the work reported in this thesis was carried out by the candidate under our supervision and has been submitted with our approval as university supervisors.

Signature..... Date.....

Dr. Willis. J. Ambusso

Department of Physics

Kenyatta University

Signature..... Date.....

Dr. Githiri J. Gitonga
Department of Physics
Jomo Kenyatta University of
Agriculture and Technology

DEDICATION

This thesis is dedicated to my entire family

ACKNOWLEDGEMENTS

This research project would not have been successful if it was not because of Gods will and favor. He held my hand and talked to me throughout the process. I therefore thank God in a special way. Secondly, my supervisors took me through every stage selflessly and tirelessly. Dr. Willis Ambusso and Dr. Githiri Githonga added value to every bit of the work done in this research project. I am very grateful for all the support and guidance from them. I am also grateful for the Geothermal Development Company (GDC) Nakuru Branch for assisting me in data collection and permission to perform this work within their area. Am also very grateful for my family who supported me in many ways in the process of doing this research work. In addition, I am thankful to my colleagues Hezekiah Cherop, Joseph Nguru, and Eric Rayora for the immeasurable support they gave me. God bless you all.

TABLE OF CONTENTS

LIST OF TABLE

LIST OF FIGURES

LIST OF APPENDICES

LIST OF ABBREVIATION, ACRONYMS AND SYMBOLS

$\mathbf{g_{obs}}$	Observed gravity data
$\mathbf{g_{abs}}$	Observed gravity data
$\mathbf{g_n}$	Latitude correction
$\mathbf{g_{fa}}$	Free air correction
h	Elevation in metres
$\mathbf{g_b}$	Bouguer slab correction
ρ	Density of rocks
TC	Terrain correction
3D	Three dimensions
2D	Two Dimensions
GPS	Global Positioning System
P	Average crustal density
N	Number of compartments of a hammer chart zone
$\mathbf{r_1}$	Inner radius of a hammer chart zone
$\mathbf{r_2}$	Outer radius of a hammer chart zone
z	Elevation difference, (mean elevation-station elevation)
CBA	Complete Bouguer Anomaly
REF	Absolute reference station
STN	Station
SI	Structural Index

ABSTRACT

Geothermal energy has become increasingly important around the world for the past few decades. This renewable energy has been utilized for electricity generation in Kenya. Before harnessing and utilizing this energy, survey of the geothermal area must be done. Moinonin has several geothermal manifestations in form of fumaroles, hot altered ground and steaming grounds among others. Even with these geothermal manifestations, gravity survey has not been done in the area. There is need to explore the area in order to ascertain the presence of a heat source and to determine its depth from the surface. Ground gravity measurements of 132 gravity stations in Moinonin, west of Lake Baringo were carried out to image the subsurface geology and map out areas associated with high temperature intrusive bodies. At each station, elevation and location coordinates were measured using a Global Positioning System (GPS). The time at which the measurement in each station was carried out was also recorded. Measurement of the gravitational attraction exerted by the earth at the measurement station on the surface was done using a gravimeter with an accuracy of ± 0.1 mGal. Data reduction on the gravity data was done to take care of corrections. Gridding was then done using surfer software and bouguer anomaly map plotted. Profiles were drawn on the contour map along the discerned anomalies. Modeling was then done using Grav2dc software, along the selected profiles. This was to attempt to identify possible fault lines, presence and depths of anomalous bodies that may be heat sources. Gravity highs were observed to be widely spread on the northern and the southern part of the area. 2-D Euler deconvolution along the profiles shows that there are fault lines in Moinonin area, which form conduits for thermal fluid flow. The models developed show heat sources protruding up to between 500m and 700m below the surface. The density contrast of the models was between 0.2475gcm^{-3} and 0.2850gcm^{-3}, which is the density of an intrusive igneous rock. It was therefore concluded that there are thermal bodies in Moinonin. This confirms that the area has high potential for electricity production and there is need for exploration. The heat should be tapped to generate electricity. Other methods can now be used for confirmation and verifications of the heat reservoir.

CHAPTER ONE

INTRODUCTION

1.1 Background to the study

Gravity surveys shed light on the structure and physical properties of geothermal fields. Hydrothermal activity around the Moinonin geothermal prospects is manifested by extensive occurrence of fumaroles, hot springs, altered grounds and thermally anomalous ground-water boreholes. In spite of the manifestations, gravity survey has not been carried out in Moinonin and therefore the structure and the physical properties of the sub surface of the area are not known. According to Dunkley *et al.* **(**1993**)**, few gravity measurements have been performed in the Lake Baringo area by research groups. The Gravity survey information on the area is very crucial to all interested parties. Borehole drillers lack information about geothermal bodies in Baringo. One of the boreholes, the Chepkoiyo borehole, which was drilled in April 2004, self-discharged water at 98^{o}C (local boiling point). Kenya is endowed with vast geothermal resource potential along the wide Kenya Rift valley that transects the country from North to South. Exploration by Kenya Electricity Generating Company Ltd (KenGen) and Geothermal Development Company Ltd (GDC) in collaboration with the Ministry of Energy (MoE) reveals that geothermal potential exceeds 10000 MWt and is capable of meeting all of Kenya's electricity needs over the next 20 years. Out of this potential, about 580 MWt and 18 MWt are being utilized for indirect and direct uses respectively. The Least Cost Power Development Plan (2008-2028) prepared by the Government of Kenya indicates that geothermal plants have the lowest unit cost and therefore suitable for base load and thus, recommended for additional expansion. Electric power demand in Kenya currently stands at over 8%

annually. In order to meet the anticipated growth in demand, more research has to be done. Lake Baringo Geothermal Prospect is one of the several important areas on the Kenya Rift floor that are associated with possible occurrence of geothermal resource.

1.2 Regional geological setting

Moinonin area is an unexploited geothermal resource located in the western part of the lake Baringo. Lake Baringo is located within the eastern floor of the Kenyan rift valley, which is part of the East African Rift System. It is bounded by latitudes $0^0$30'N and $0^0$45'N and longitudes $35^0$59'E and 36^0 10'E. Figure 1.1 shows the regional setting of Lake Baringo.

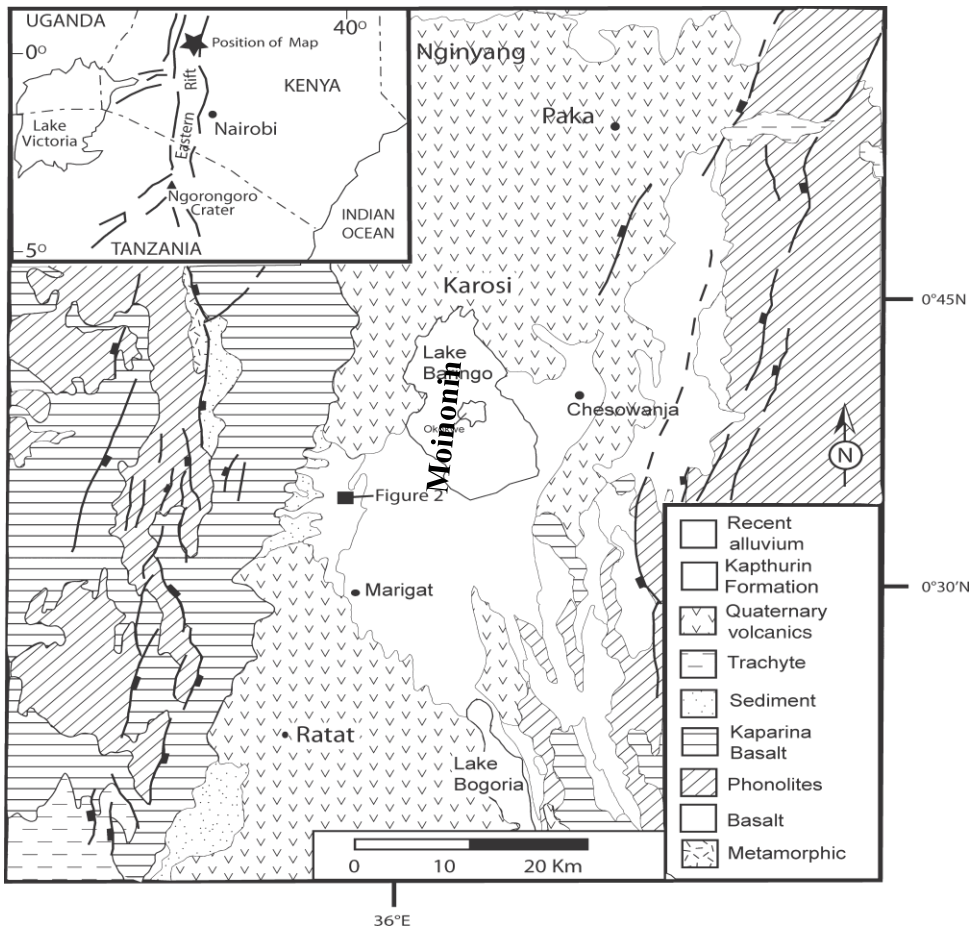

Figure 1.1 Geology of the Lake Baringo in the Eastern (Gregory) Rift, Kenya (adapted from Chapman & Brook, 1978)

Lake Baringo is one of the important areas on the Kenyan rift floor that is associated with possible occurrence of geothermal resource. The Tugen hills, an uplift fault block of volcanic and metamorphic rocks lies west of the lake. The Laikipia escarpment lies to the East. The Baringo trachyte was described by Martyn (1969) as the 'Lake Baringo Trachyte'. The Baringo trachyte outcrops over 12km^2 west of Kampi ya Samaki. It was the major source material for artifacts found in Kapthurin basin (Tallon, 1978). The striking appearance on aerial photographs is due to lineaments, which reflect pressure ridges resulting from the congealing of highly viscous lava. The trachyte is fine grained, black, streaked with green and locally speckled, an expression of glomerophyric clusters of dark minerals. Sanidine forms about 60% of the mode: otherwise aegirine-angite, aenigmatite and zeloilites are commonly observed in this section (Dagley *et al.*, 1978).Thin basalt flows occur on the west side of the lake (Truckle, 1977) forming the greater part of the outcrops which Martyn (1969) referred to 'Basalts of Nginyang type'. They are well exposed on the lakeshores promontories between Kampi ya Samaki and west Bay, and further north at Logoratabim. The Baringo basalts are typically weather black with a rough texture due to vascularity. Columnar or rough blocky jointing is usual in the area. The lake has several small islands, the largest being Olkokwe island which is an extinct volcanic center related to Korosi volcano, north of the lake.

1.3 Statement of research problem

Moinonin has several geothermal manifestations in form of fumaroles and hot springs that discharge along the shoreline of the lake. Not much research has been done in the area to determine the presence and location of a geothermal body. Establishing the presence and location of a geothermal body in Moinonin area would be welcome

news to the locals, scholars and companies who exploit geothermal resources. The final process of harnessing the geothermal resource would improve economic activities in the area and create technical jobs and opportunities. Geothermal power doesn't rely on the weather and therefore it is cost effective and reliable. Due to erratic and unpredictable weather patterns and climate change globally, the main source of power which is dependent on the water levels in the dams has been unreliable. The power supplier has had to resort to power rationing and producing power using petroleum run generators which is not environmentally friendly. This is also expensive and the extra cost of production has always been passed on to the consumers. In Kenya, the installed capacity of power generation has not increased to match the demand growth thus emergency power has been procured to satisfy big demands. In recognition of the importance and reliability of geothermal power and the energy requirement to meet vision 2030, the government has embarked on an ambitious generation expansion plan to increase the installed capacity through enhanced geothermal development (Simiyu, 2010).It is therefore necessary to carry out research in this region to determine the viability of geothermal resource and recommend exploitation to supplement power supply.

1.4 Objectives of the research project

1.4.1 General objective

To study the extent of gravity highs in Moinonin area Lake Baringo, and determine whether they could be possible sources of geothermal energy.

1.4.2 Specific objectives

The specific objectives of this study were;

i. To carry out ground gravity measurements in Moinonin area.

ii. To carry out data reduction and processing of the gravity data.

iii. To model bodies with density contrast of possible heat sources.

1.4.3 Rationale of study

Insufficient energy supply is still a major impediment to economic growth in Kenya. Development in the economy is anchored on the provision of reliable, sustainable and environmentally friendly source of energy. Extensive faulting accompanied by block tilting characterizes the terrain at the western side of Lake Baringo which includes Moinonin area. These form numerous N-S ridges and fault scarps. According to Baker and Wohlenberg (1971), Baker (1986) and Baker *et al*. (1972, 1988), this complex network of faults and fractures suggests that tensional strain oblique to the primary rift axis is still occurring and there is need to make a deliberate effort to harness geothermal potential in Lake Baringo.

CHAPTER TWO

LITERATURE REVIEW

2.1 Geothermal system

A geothermal system is made up of four main elements namely, a heat source, a reservoir, fluid which is the carrier that transfers the heat and fluid path ways (for example faults and fractures). Parameters that characterize a geothermal system are temperature, porosity, permeability and chemical composition of the fluid. The main interest is in areas where we get high temperatures, high pressure, high porosity and good permeability and low content of dissolved solids and gases in the water. Geothermal resource is associated with an area of Quaternary volcanism in which rhyolites dominate. Geophysical exploration for the resource during the early stages of development included dipole, Schlumberger, electromagnetic, head-on, gravity, seismic and magnetics and various levels of success were achieved.

It was noted that whereas resistivity was the most important in identifying the reservoirs, depth of penetration was low for dipole and Schlumberger while interpretation of head-on data was ambiguous. Gravity survey of the shallow crust is used to indicate fault zones characterized by low density (Naomi, 1981). Precision gravity surveys have been used at Olkaria Geothermal Field in 1983 to monitor gravity changes as a result of geothermal fluid withdrawal (Mwangi, 1983). A review of the observed gravity data over each benchmark indicated changes over the years during monitoring period (Marietta, 2000). The occurrence of late phases rhyolites (cementite) lavas and pyroclastic indicates the presence of shallow magma bodies since it has been established that they are products of protracted crystallization and crustal anatexis (Macdonald *et al*., 1987; Black *et al*., 1997; Omenda, 2000). Such

processes have the potential to transfer large quantities of heat to the upper crust via the shallow crustal bodies.

2.2 Key benefits of geothermal energy

Geothermal energy is competitive in terms of cost. Estimates indicate that it can even compete with large-scale hydropower (Stefansson, 1999). Geothermal power plants have near zero emissions, (true for modern closed cycle systems that re-inject water back to the earth's crust) and very little space requirement per unit of power generated (Karekezi and Kithyom,2008). This makes geothermal energy an attractive option compared to fossil fuel alternatives. Geothermal energy is not susceptible to seasonal fluctuations, and is available all year round. This is in contrast to hydroelectric power, which is affected by low rainfall and oil-fired power plants, which can be prohibitively expensive to operate when oil prices are high. Geothermal energy has other direct uses such as space heating and heating of green houses for horticultural farming (Lund *et al.,* 2005). The knowledge base on geothermal energy is growing rapidly, with a sizeable expert team present in Kenya.

2.3 Gravity method

The gravity method measures the spatial variations in the strength of the gravitational field of the earth. The underlying concept is the idea of a causative body, which is a rock of different density from its surroundings. This causative body represents a subsurface zone of anomalous mass and causes a localized perturbation in the gravitational field known as a gravity anomaly. Because the force of gravity is proportional to the mass responsible for the gravitational field and inversely proportional to the square of the distance between any part of that mass and the observation point, a local lack of normal mass (say, a thick layer of low-density

sediments instead of heavy igneous rocks of negligible porosity) will result in a local gravity low. A mass of unusually dense rock (gabbro intruding sedimentary rock or acidic volcanics) will generate gravity high.

2.4 Ground gravity survey

A wide range of geophysical surveying methods exists for exploration for geothermal energy as well as the monitoring of geothermal reservoirs under exploitation (Ndombi, 1981; Mariita, 1995; Simiyu and Keller, 1997). The type of physical property to which a method responds dictates the application. Although many of the geophysical methods employed require complex methodology and relatively complex mathematics in processing and interpretation of data derived, much information is derived from a simple assessment of the survey data. In gravity surveying, subsurface geology is investigated based on variations in the earth's gravitational field generated by differences of density between subsurface rocks. A subsurface zone whose density is different from that of the surroundings causes a localized perturbation in the gravitational known as a gravity anomaly. Volcanic centre, where geothermal activity is found, are indicators of cooling magma or hot rock beneath these areas as shown by the recent volcanic flows, ashes, volcanic domes and abundant hydrothermal activities in the form of fumaroles and hot springs. Gravity studies in volcanic areas have effectively demonstrated that this method provides good evidence of shallow subsurface density variations, associated with the structural and magmatic history of a volcano (Ndombi, 1981). There is a correlation between gravity highs with centers of recent volcanism, intensive faulting and geothermal activity.

2.5 Gravity surveys in Kenya

According to Mwangi (2005), Kenya is one of the African countries that tap energy from the crust of the earth for electric power generation. Geothermal investigations started as long ago as 1956 when exploratory drilling was undertaken by a consortium of companies. It is observed that Kenya is endowed with vast geothermal resource potential along the wide Kenya rift valley that transcends the country from north to south as shown in figure 2.1. According to Simiyu (2010), Kenya electricity generating company limited (KenGen) and geothermal development company (GDC) in collaboration with ministry of energy have undertaken a detailed surface studies of most of the prospects in the Kenya rift which comprises Suswa, Longonot, Olkaria, Eburru, Menengai, Lakes Bogoria and Baringo, Korosi and Paka volcanic fields. Kyalo (2011) used the gravity survey in Arus area of Lake Bogoria where he found bouguer anomaly of approximately 40mGals along the north south of the lake.

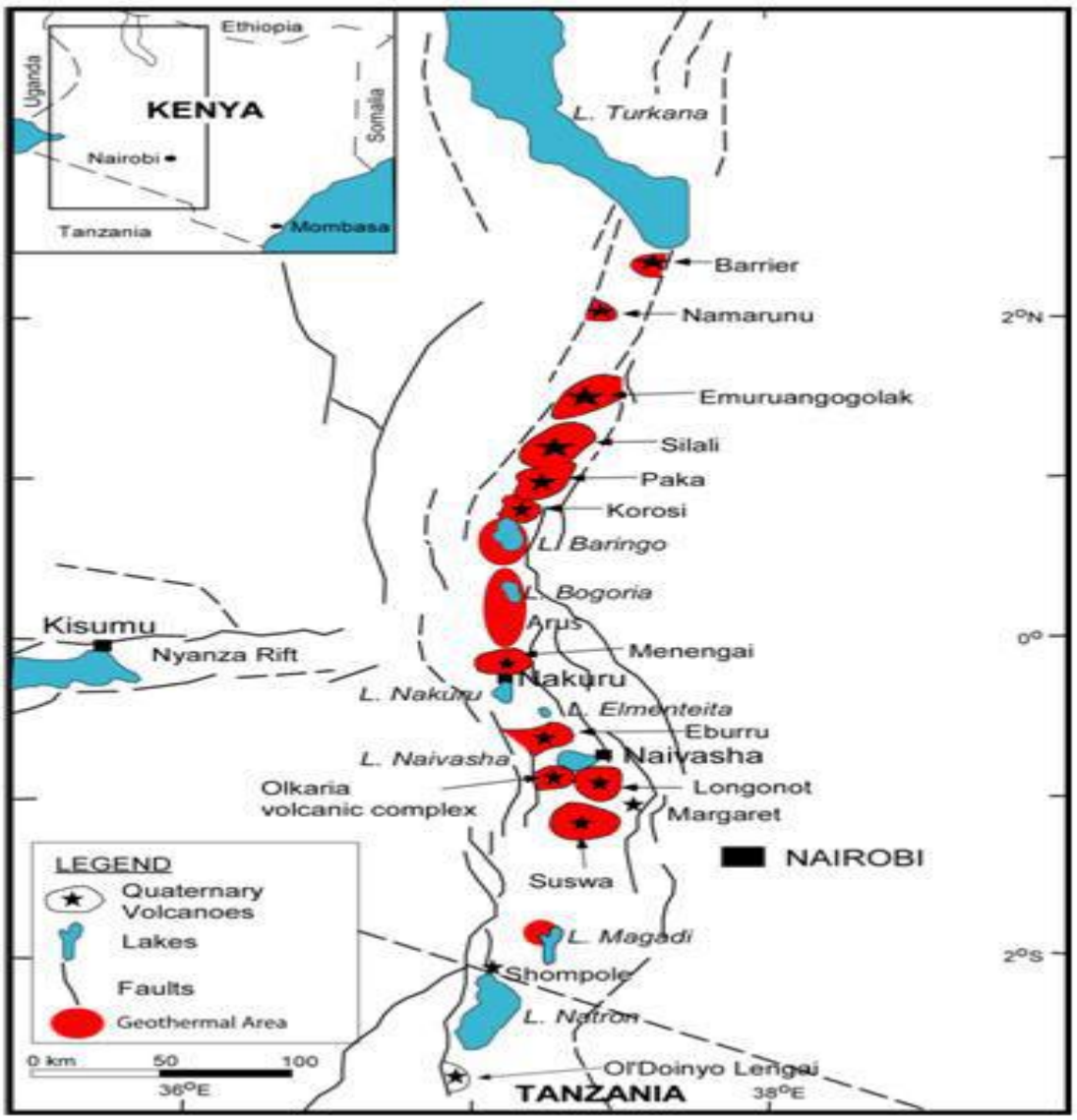

Figure 2.1 Map showing Lake Baringo and other locations of the geothermal fields and prospects in Kenya (Omenda, 2007)

2.6 Previous geophysical work in Lake Baringo

Geophysical methods for geothermal exploration have been carried out around the prospects area since early 1980. According to Dunkley *et al.* (1993), a few gravity measurements had been performed in the Baringo area by research groups. The techniques that have been applied include seismic, gravity, magnetic and resistivity surveys. In 2004, KenGen carried out a gravity survey (Lagat *et al.*, 2005) in this area. Data from this investigation was processed and corrected for terrain and drift before

compiling a contour map for the Baringo region. Gravity highs are evident to the western and northern rims of Lake Baringo. The National Oil Corporation of Kenya collected aeromagnetic survey over the whole rift zone at 300m above ground in 1987. A qualitative examination of this data by Mariita (2003) indicated positive anomalies for the north rift's volcanic centers superimposed over a negative regional background. Moderate values were recorded in the central region of the prospect area, while the lowest values delineate the sediments surrounding the lake.

Mariita and Kilele (1989) demonstrated that the Ministry of Energy of Kenya carried out a few schlumberger resistivity measurements north of Baringo in the late 1980s. This was part of a reconnaissance study for geothermal potential in the region. An analysis of the soundings from these work indicated a discrete anomaly less than 20 Ωm at depths of 1000m lodged northwest of Lake Baringo. Based on this data, KenGen in 2004 increased the number of stations to substantially mirror the resistivity structure of the Baringo prospect. Conversely, the limited number of soundings could not offer a definite image of subsurface structures and formations.

CHAPTER THREE

MATERIALS AND FIELD METHODS

3.1 Introduction

Gravity surveys shed light on the structure and physical properties of geothermal fields. There are broad ways of geophysical surveying that makes use of natural fields of the earth. The natural fields make use of gravitational, magnetic, electrical and electromagnetic fields of the earth. These methods try to search for local perturbations in the natural occurring fields that may be caused by geological features of economic or other interest. These natural field methods provide information on earth properties to significantly greater depths and are logistically simpler to carry out compared to artificial methods.

3.2 Gravity instruments

3.2.1 Sodin gravimeter

One of the common unstable instruments used to measure relative gravity measurement is the sodin gravimeter. The mechanical arrangement provides the instability with two springs, one acting as the measuring device and the other alters the level of the reading range. It has an accuracy of $\pm$0.1 gu. It pivots a small mass on a torsion fiber against the torque provided by stretching a calibrated quartz spring. The main shortcoming is the drift due to imperfect elasticity of the springs and temperature changes during the study period of the day. This drift is monitored by repeated meter readings at base stations throughout the day.

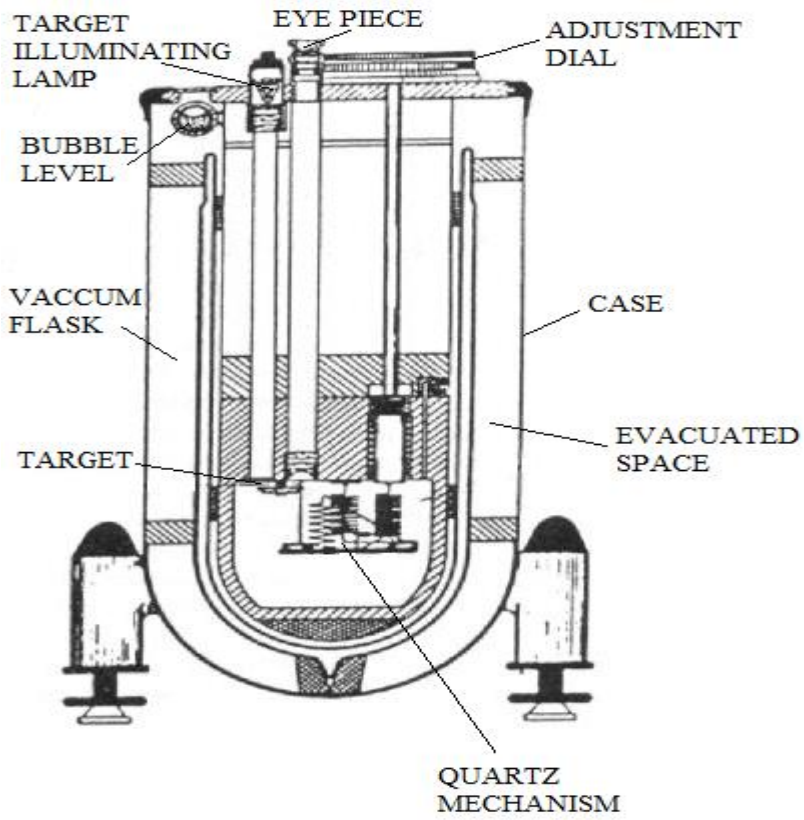

Figure 3.1 Schematic diagram of the Sodin gravimeter

Figure 3.2 The Sodin gravimeter

3.2.2 Global Positioning System (GPS)

This is a satellite navigation system used to locate points on the earth surface. The GPS concept is based on time and the known position of specialized satellites. The satellites carry very stable atomic clocks that are synchronized with one another and to ground clocks. Any drift from true time maintained on the ground is corrected daily. Likewise, the satellite locations are known with great precision. GPS satellites continuously transmit their current time and position. A GPS receiver monitors multiple satellites and solves equations to determine the precise position of the receiver and its deviation from true time. At a minimum, four satellites must be in view of the receiver for it to compute four unknown quantities (three position coordinates and clock deviation from satellite time).

Figure 3.3 Illustration of GPS receiver

3.3 Field stations

3.3.1 Area topography

The Garmin GPS receiver was used to establish coordinates and elevation of each station. The area is generally flat with elevation between 960m and 1200m above sea level. Surfer software was used to draw a contour map showing the topography of the area as in figure 3.4.

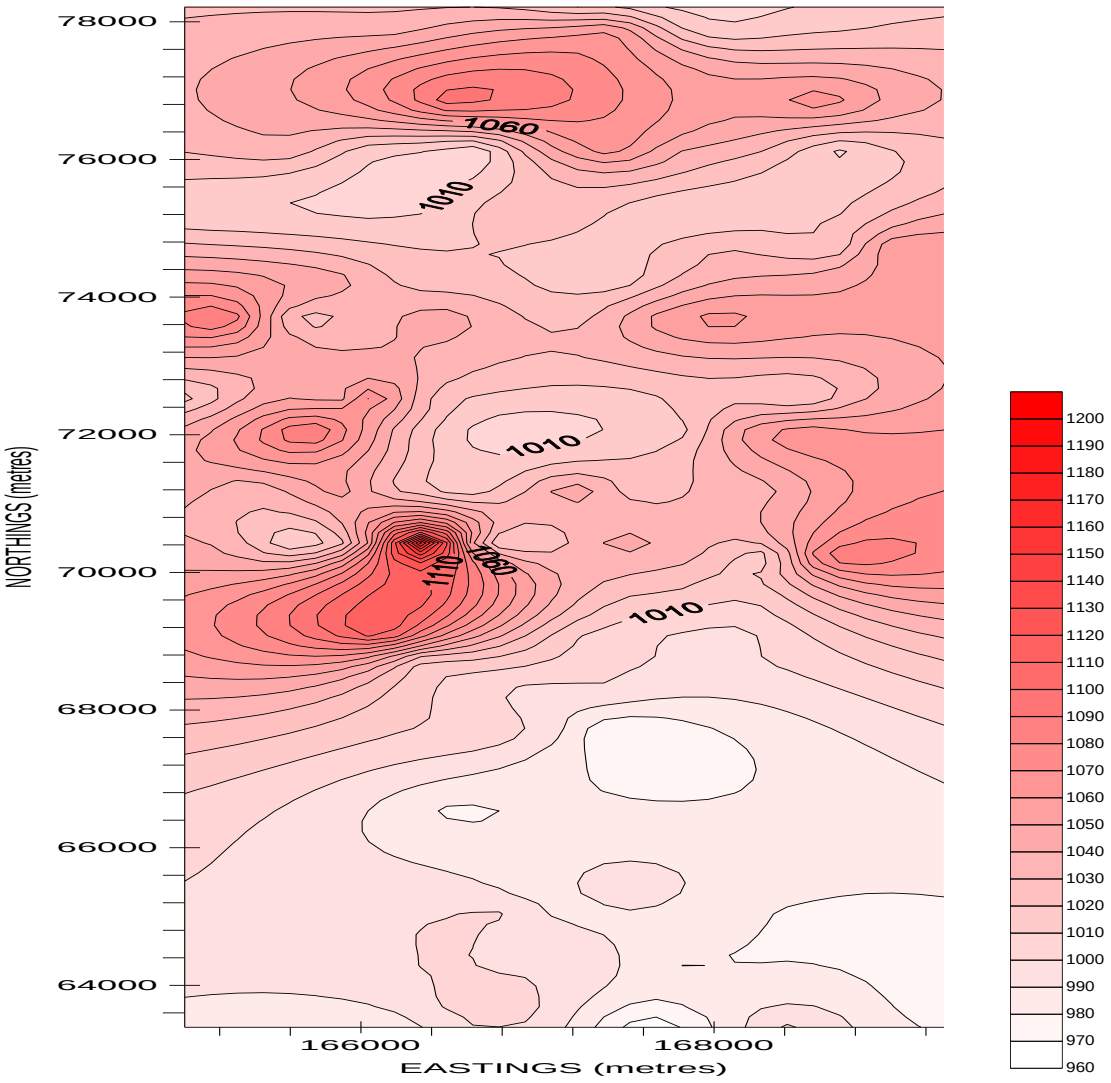

Figure 3.4 Area topography of Moinonin

3.3.2 Field stations

The survey covered an area of about 48km^2. The gravity stations were along lines called profiles. 23 profiles spaced between 300m and 1000m apart were used in the collection of data. Each profile had a total length of between 500m and 4000m. 132 gravity intensity stations were measured with a spacing of between 200m and 1000m intervals along each line as shown in figure 3.5. At each station the latitude, longitude, elevation, Grid Easting and Grid Northing was obtained using a Global Positioning System.

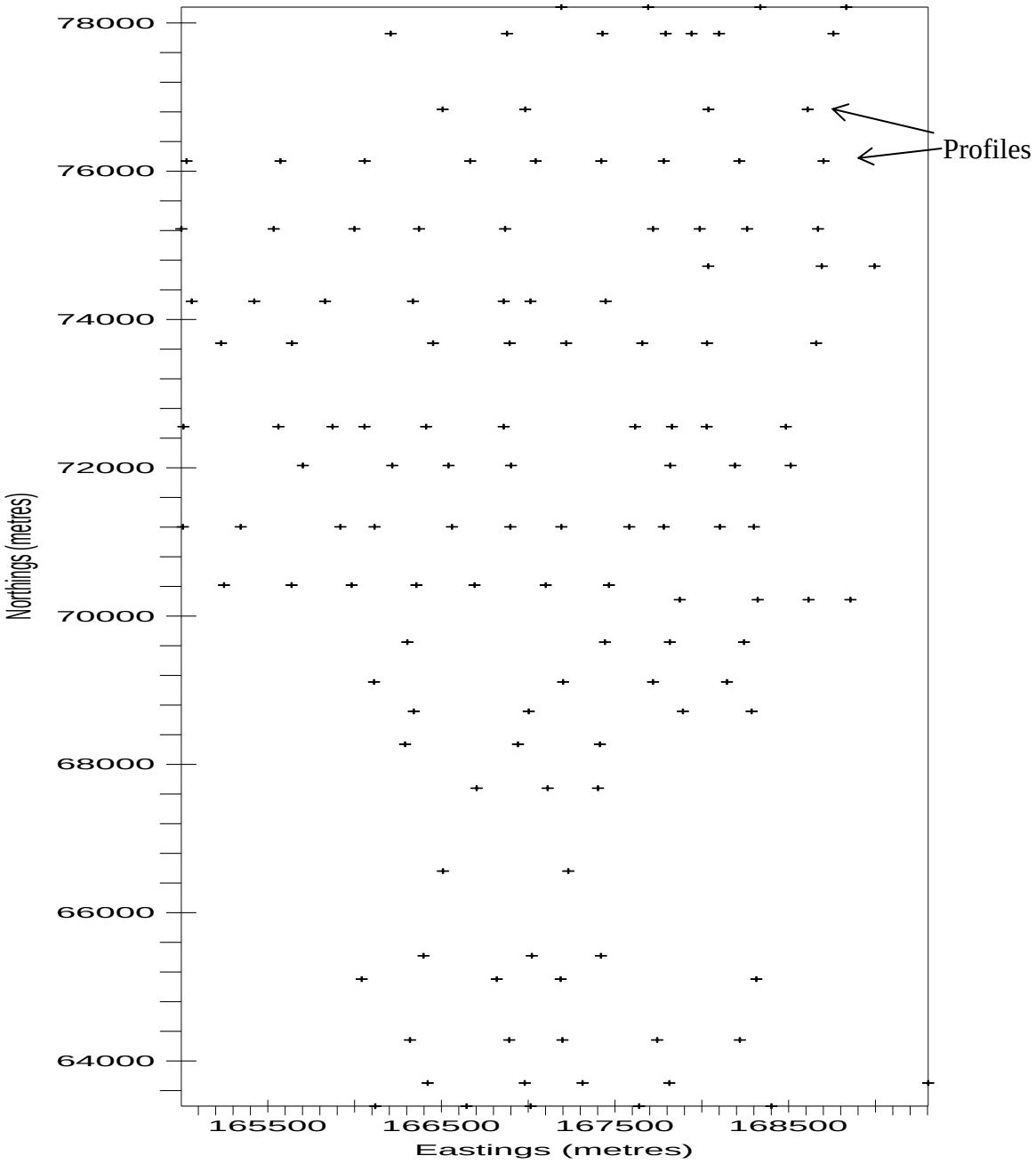

Figure 3.5 Spatial distribution of gravity stations

3.4 Data acquisition

The elevation and the location of the survey area were measured using the GPS. Once a survey area was located using the GPS, the gravimeter was leveled using the adjustable screws at the base of the meter. The dial reading of the gravimeter was taken and recorded on the field notebook. Time was also measured using a watch. A

base station was established at a convenient point in the site and was preoccupied at regular intervals during the survey day. The preoccupied base station was to check on the drift of the gravimeter. Readings of the gravimeter were taken along each profile along the Northings. The gravimeter measured the differences in gravity from one station to another. All the measurements were recorded in field book for each day of survey. Appendix1 and 11 show all the raw data collected from the study area for the gravity measurement stations and base stations respectively.

CHAPTER FOUR

DATA REDUCTION AND PROCESSING

4.1 Introduction

Before the results of a gravity survey can be interpreted, it is necessary to correct for all variations in the Earth's gravitational field, which do not result from the differences of density in the underlying rock. These include drift correction, latitude correction (g_n), free air correction (g_{fa}), bouguer slab correction (g_b) and terrain correction (TC).

4.2 Data reduction

Data reduction is the process of removing all variations in the earth's gravity field due to other factors other than the underlying rocks. Observed gravity (g_{obs}) is the gravity reading observed at each gravity station after corrections were applied for instrument drift. These corrections were assumed to have accurately accounted for the variations in gravitational acceleration they were intended to account for. Any remaining variations in the gravitational acceleration associated with the Terrain Corrected Bouguer Gravity were assumed to be caused by geologic structure of the study area.

4.2.1 Drift correction

Gravimeters are sensitive instruments. Temperature changes and elastic creep in the springs cause readings to change gradually with time. This drift was monitored by repeating readings at base station at different times of day, every 2-3 hours. The collected base station gravity meter readings were then plotted against time. A line is fitted to the readings to provide time rates of drift for the correction of the remainder of the observations, as shown in figure 4.1 below.

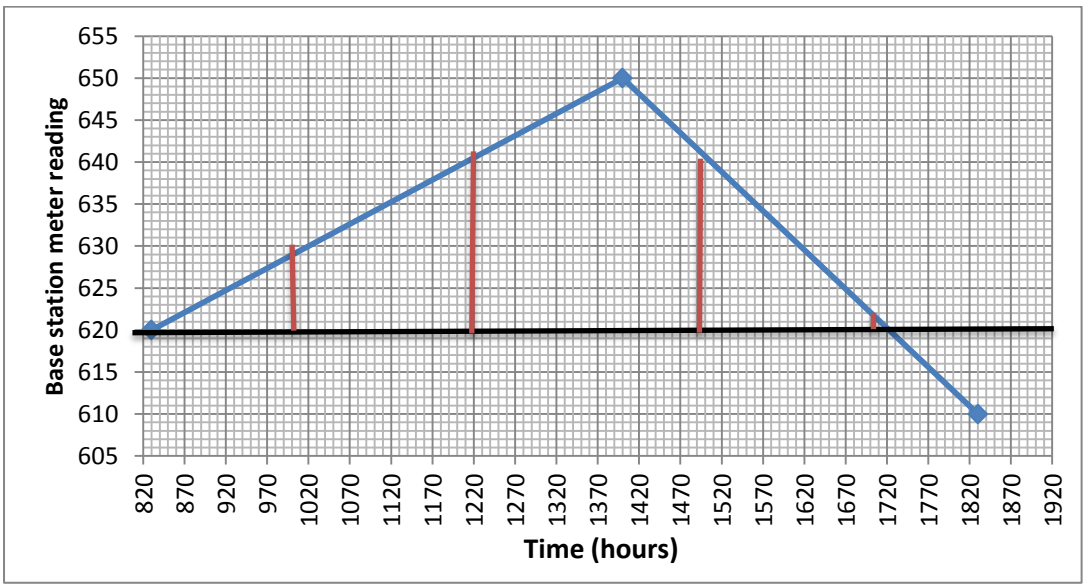

Figure 4.1 Drift curve for first day.

Instrument drift correction for each station was then estimated from drift curves. For instance at 1020 hrs, the drift is 10. The drift was subtracted from the station dial reading to give the corrected station dial reading. For instance, for the station code KPS001,

623-20 = 613.

The difference between the corrected station dial reading and the dial reading of the reference station was multiplied with the instrument calibrated constant which is 0.10062.

For station code KPS001,

(613 – 602) × 0.10062 = 1.10682.

This product was then added to the absolute gravity of the reference station to give the observed gravity of the station under study. For station code KPS001,

977641 +1.10682 = 977642.41.

The process was repeated for all the gravity stations and Appendix III shows the drift corrections for each day and the consequent observed gravity for each station.

4.2.2 Latitude correction (g_n)

Gravity varies with latitude because the earth is not a perfect sphere and the polar radius is smaller than the equatorial radius. Also, the effect of centrifugal acceleration is different at the poles versus the equator. Thus, gravitational acceleration is larger at the poles than at the equator. According to woollard *et al* (1980), the relationship that fully expresses the correction that accounts for Earth's elliptical shape and rotation is as shown in equation 1;

$$gn = 978031.85(1.0 + 0.005278895 \sin 2\theta + 0.000023462 \sin 4\theta) \quad (1)$$

Where θ is the latitude. Latitude value θ, for each station obtained from the GPS was substituted in equation 1 to obtain the latitude correction (g_n) data as shown in appendix IV.

4.2.3 Free air anomaly (g_{fa})

A high station has gravity that is low since it is farther from center of Earth. According to Woollard et *al* (1980), the free-air correction equation as in equation 2 was to account for gravity variations caused by elevation differences in the observation locations.

$$gf_a = 0.3086h \quad (2)$$

Where h is the elevation in metres, at which the gravity station is above the datum (typically sea level). The elevation for each station obtained from the GPS was substituted in the equation 2 to obtain the free air anomaly (g_{fa}). For the station code KPS001,

$$g_{fa} = 0.3086 \times 1024 = 316.01$$

The process was repeated for each station to obtain data as shown in appendix IV.

4.2.4 Bouguer slab correction (g_b)

Excess mass between the reading elevation and the datum elevation makes the gravity reading higher. According to Woollard *et al* (1980), the corrections that account for excess mass underlying observation points located at elevations higher than the elevation datum (sea level or the geoid) is removed using the gravity international equation 3;

$$g_b = 0.04193\rho h \qquad (3)$$

Where ρ is the average density of the rocks underlying the survey area and h the elevation of the area. The average density of the crustal rocks is 2.67g/cm^3 according to Woollard et *al* (1980). Substituting this average value of the density and the elevation (h) for each station in equation 3, the bouguer slab correction for each station was obtained as shown in appendix IV. For station code KPS001,

$$g_b = 0.04193 \times 2.67 \times 1024 = 114.64$$

4.2.5 Terrain correction (TC)

The presence of terrain always reduces the value of gravity. The correction shown in equation 4 was to account for variations in the observed gravitational acceleration caused by variations in topography near each observation point. A circular graticule known as the hammer chart was used to obtain the mean elevation for each compartment.

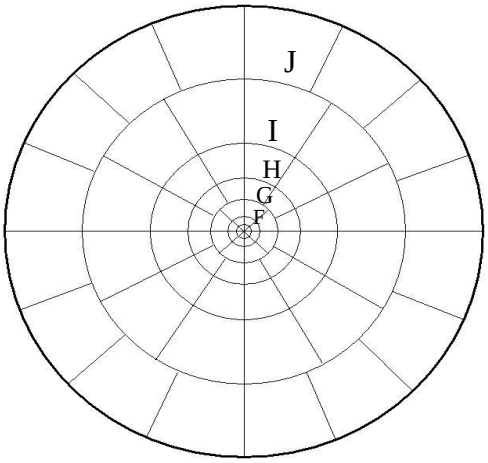

Figure 4.2 Schematic diagram of the hammer chart

The graticule was laid on the topographic map with its center on the gravity station and the average topographic elevation of each compartment determined. The elevation of the gravity station is subtracted from these values to obtain the elevation difference (z) and the gravitational effect of each compartment is determined using the international gravity formula (Woollard *et al*., 1980) for the gravitational effect of a sector as in equation 4;

$$g_{TC} = 0.04191 \frac{\rho}{n}\left(r_1 - r_2\right) - \sqrt{\left(r_1^2 + z^2\right)} - \sqrt{\left(r_2^2 - z^2\right)} \qquad (4)$$

where

ρ -average crustal density

n –number of compartments in a zone

r_1 - inner radius of a zone

r_2 -outer radius of a zone

z- Elevation difference, (mean elevation-station elevation)

Table 4.1. Table of quantities for Terrain correction

Zone	r_1	r_2	n
F	390.1	894.8	8
G	894.8	1529.4	12
H	1529.4	2614.4	12
I	2614.4	4468.8	12
J	4468.8	6652.2	16
K	6652.2	9902.5	16
L	9902.5	14740.9	16

From the results as shown in appendix IV, the terrain effects are observed to be low due to the subdued topography of the area.

4.2.6 Complete Bouguer Anomaly (CBA)

The main end product of gravity data reduction is the Complete Bouguer Anomaly (CBA). The CBA should correlate only with lateral variations in density of the upper crust and is of most interest to applied geophysicist and geologists. The Complete Bouguer Anomaly was obtained by making all reductions on the observed data. Using the international gravity equation (Woollard et al., 1980), the latitude correction, the free air correction, the bouguer slab correction and the terrain correction was done on the observed gravity data as in equation 5;

$$gt = gobs - gn + 0.3086h - 0.04193\rho h + TC \quad (5)$$

Free air correction and terrain correction were added to the observed gravity while latitude correction and bouguer slab correction were removed from the observed gravity. For station code KPS001,

$g_b = 977642.41 - 979956.55 + 316.01 - 114.64 + 0.1941 = -1542.62\,\text{mGals}$

Appendix IV shows the CBA for all gravity stations.

4.3 Data processing

Once the basic latitude, free-air, Bouguer and terrain corrections were made, an important step in the analysis remains. This step, called regional-residual separation, is one of the most critical. Bouguer anomaly fields are often characterized by a broad, gently varying, regional anomaly on which may be superimposed shorter wavelength local anomalies. Usually in gravity surveying it is the local anomalies that are of prime interest and the first step in interpretation is the removal of the regional field to isolate the residual anomalies. Direct and mathematical estimates were used to remove this regional trend from the profiles. The corrected gravity data from the survey area was then processed to facilitate interpretation. This was done by plotting a gravity contour map using the complete gravity anomaly and the station coordinates from appendix IV and figure 4.3 was obtained. Surfer software was used in the drawing of these contours. Profiles were then drawn across the gravity anomaly regions. The profiles were digitized to obtain data that was used to make detailed study of the areas along the profile. Euler deconvolution was used to provide information on the presents of fault lines as areas of discontinuity and give an indication of the presents of shallow and deep anomalous bodies along the profiles. Anomalous regions were discerned from the gravity contour map as shown in figure 4.3 below;

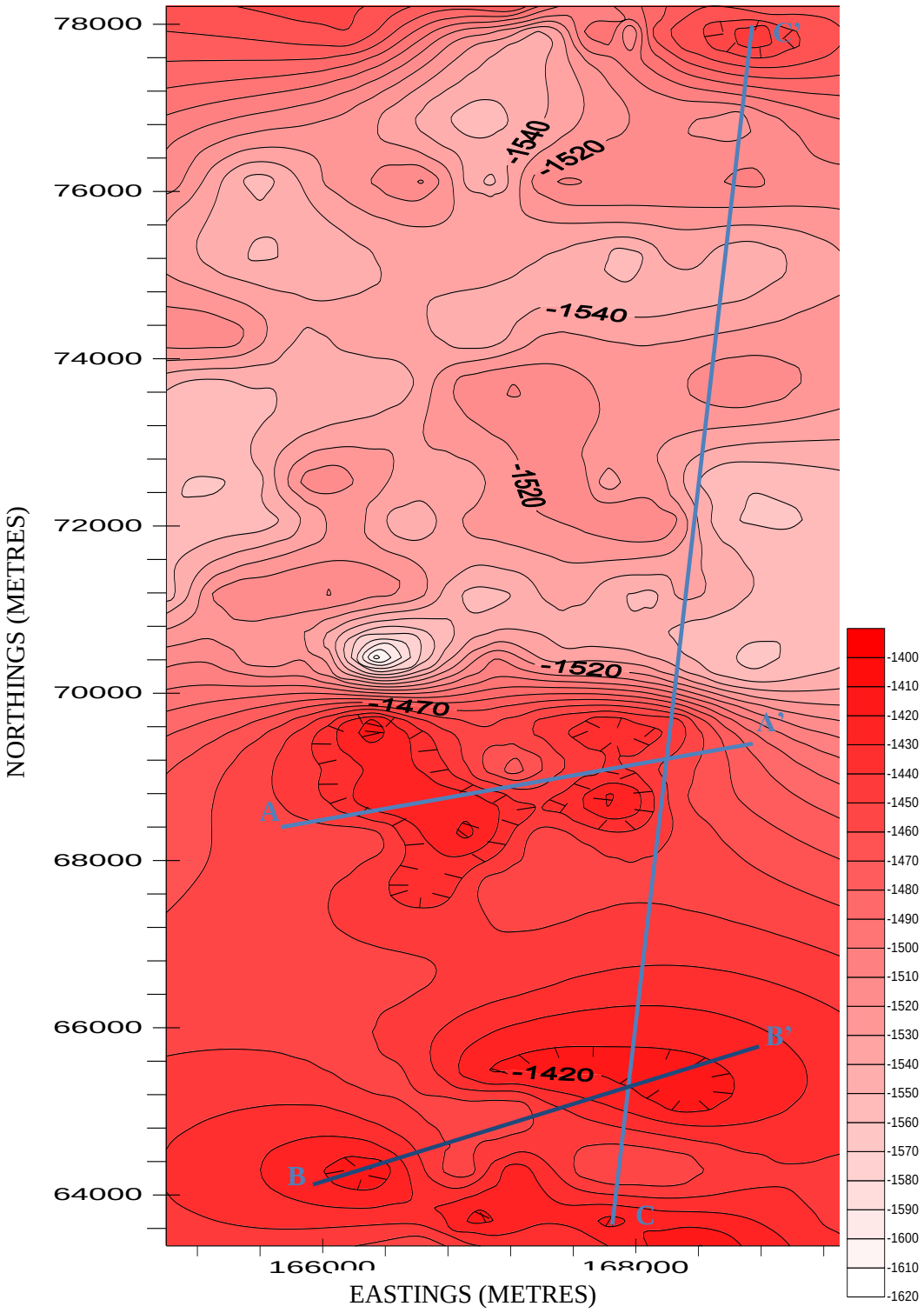

Figure 4.3 Gravity anomaly of Moinonin area.

CHAPTER FIVE

DATA ANALYSIS AND INTERPRETATION

5.1 Introduction.

In this research study, profile and contour mapping was adopted in data presentation. From contour maps and 2D models, interpretation was made based on the distribution of gravity intensities in the study area. The gravity data was then analyzed via a suite of qualitative and quantitative methods and interpreted for determination of subsurface structures that act as conduits for the flow of geothermal water to the surface. Qualitative interpretation relied on spatial patterns that can be recognized in the data. This sought to identify the presence of faults, dykes, lineaments and folds. Intrusive bodies are often recognized by virtue of the shape and amplitude of their anomalies. Qualitative interpretation was complemented with several forms of quantitative interpretation that seek to provide useful estimates of the geometry, depth and densities of the gravity anomaly source.

Broadly categorized as curve matching or forward modeling, quantitative technique rely on the notion that simple geometric bodies, whose gravity anomaly can be theoretically calculated, can adequately approximate gravity of more complex bodies. In processing, interpreting and presenting data from this study, specialized software surfer 8 (golden software) and Grav2dc for modeling were used. Grav2dc calculates the anomalous field caused by an assemblage of 2-dimentional gravity bodies defined by a polygonal outline.

5.2 Qualitative Interpretation

The use of the surfer software and excel software assisted in developing a qualitative interpretation of the results. The profiles selected pass through areas of interest, which

majorly were areas of gravity highs. The golden surfer software was used to slice and digitize the profile to provide data that was analyzed and used to make the qualitative analysis. Euler deconvolution is a program within surfer software. It turns the gravity field measurements into estimates of gravity source body location and depth. The method is applied to survey profile data subset extracted using a moving window. In each window Euler equation is solved for source body coordinate. The source body geometry is specified by structural index SI. Euler deconvolution is only valid for homogeneous functions. A function f(v) of a set of variables v = (v1, v2,...) has a degree of homogeneity n, if;

$f(tv) = t^n f(v)$

where t is a real number. If f has a differential at v, then;

$v \nabla_v f(v) = nf(v)$

This is Euler's equation according to Stavrev et al (2007). The Euler deconvolution relies on solving it in appropriate cases. A field F which may be expressed in the form;

$F = A/r^N$

will be homogeneous of degree –N. For convenience the Structural Index (SI) is defined as N (= -n, i.e. the negative degree of homogeneity).

5.2.1 Selection of profiles

The profiles selected were in such a way that they majorly pass through the regions of gravity highs. The profiles AA' and BB' were cutting though the southern region which is predominantly of gravity high. The profile CC' passed through a wider region covering both gravity highs and gravity lows. Profile CC' also cut the two

profiles, AA' at around 2080m and BB' at around 2300m. Appendix V shows all the data for the profiles used in this study

5.2.2 Gravity profile AA'

The profile AA' as in figure 4.3 is about 3500m long and slightly slanting along the North West direction. Using surfer software, the profile was digitized, sliced and data scattered to plot curves of the profile trend. Figure 5.1 shows the profile with a regional trend.

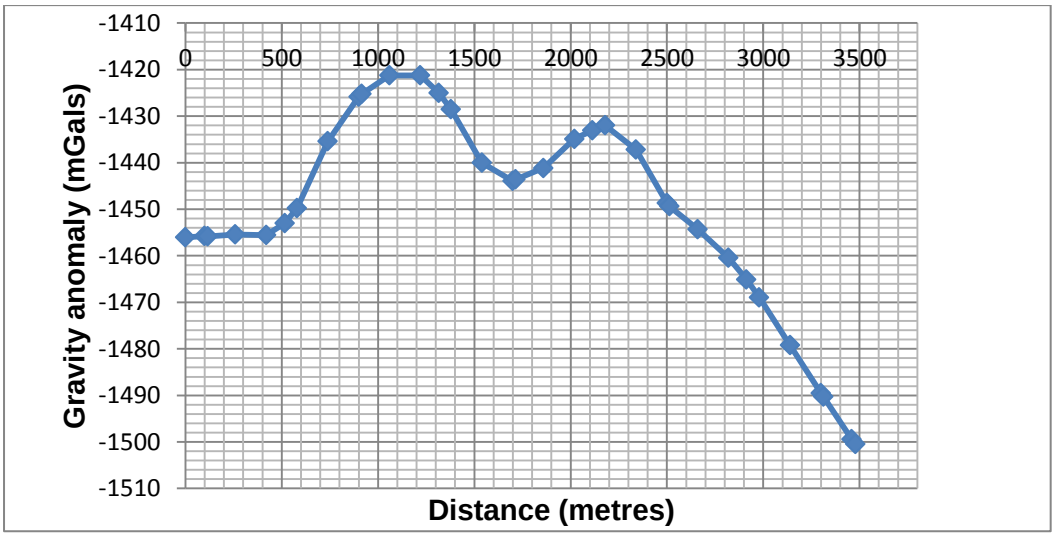

Figure 5.1 Profile AA' with regional trend

The regional trend was removed to obtain figure 5.2, which is without the regional trend.

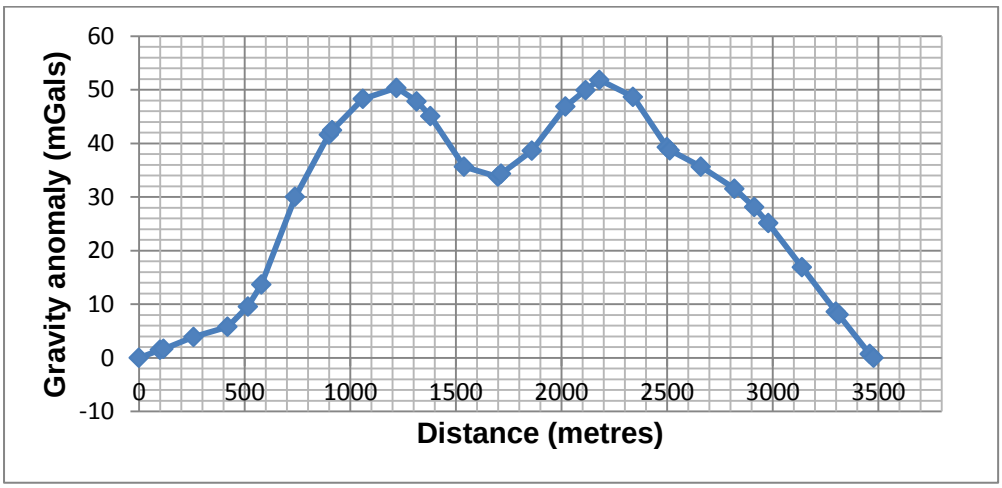

Figure 5.2 Profile AA' without regional trend

The gravity anomaly increases up to a maximum value at 1200m and 2200 m along the profile.

The data from the profile was also analyzed using Euler deconvolution. The Euler deconvolution was used to discern fault lines, causative deep and shallow bodies along each profile as shown in figure 5.3.

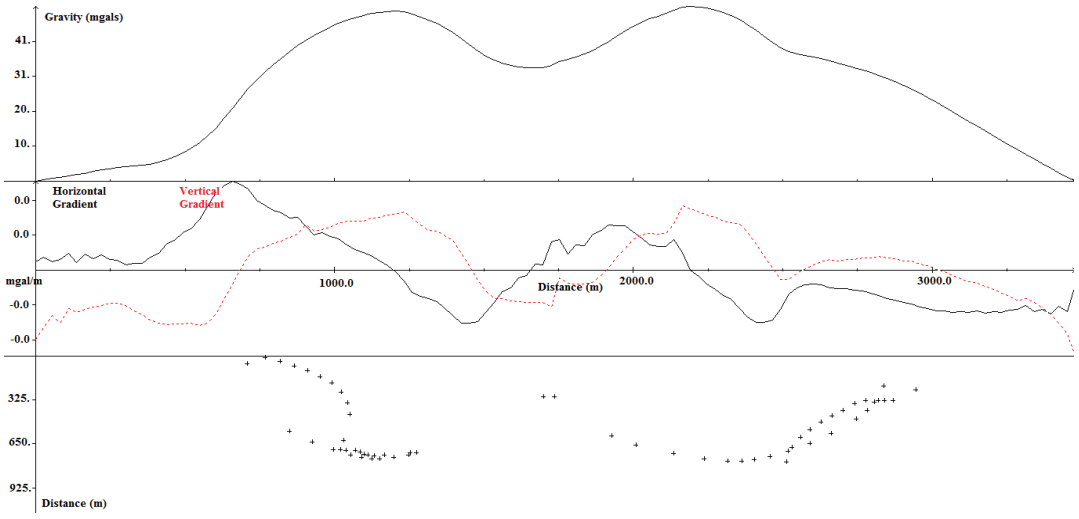

Figure 5.3 Euler deconvolution of profile AA' data

There are deep causative bodies at various points along the profile. An anomaly was observed to be between 800m and 1250 m at a depth of between 350m and700m and

between 2100m and 2500m at a depth of between 350 and 700m. It was also observed that there is shallow causative body at 750m at a maximum depth of 200m and between 2750 and 3000m at a depth of 300m. A discontinuity, which may suggest Fault lines were also observed at between 0m and 700m and between 1200m and 1700m along the profile.

5.2.3 Gravity Profile BB'

The profile BB' as shown in figure 4.3 is about 4000m long and along the North -East direction as shown in. Using surfer software, the profile was digitized, sliced and data scattered to plot curves of the profile trend. The figure 5.4 shows the profile data scattered on a grid.

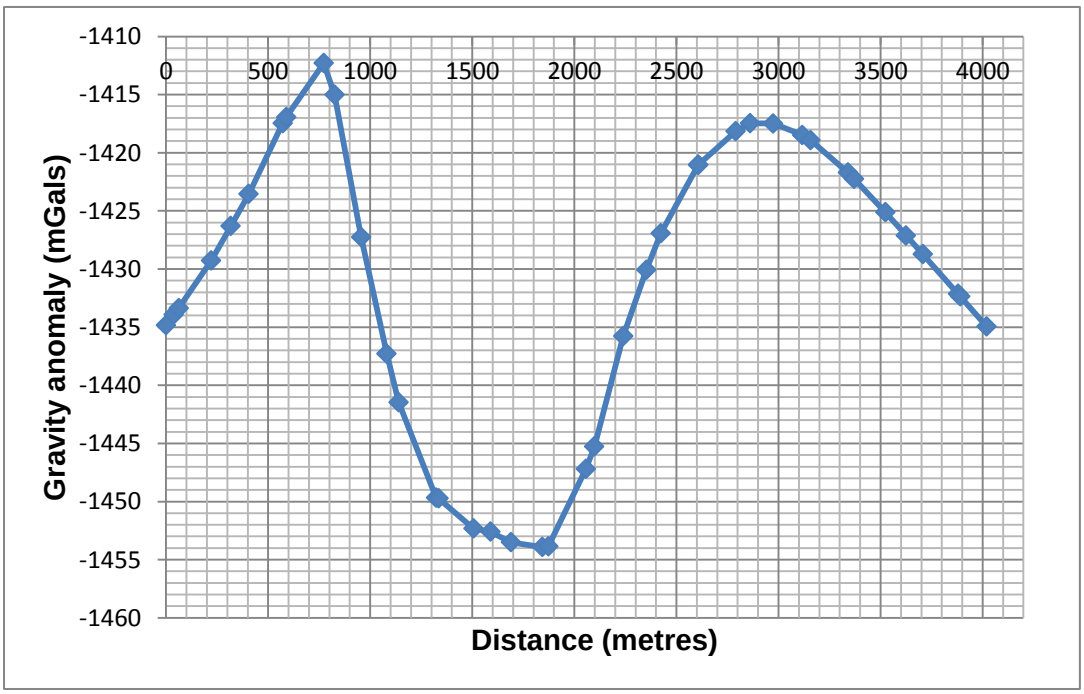

Figure 5.4 Profile BB' with regional trend

There is a small regional trend that is observed along the profile. The regional trend was removed and figure 5.5 shows the profile without the regional trend.

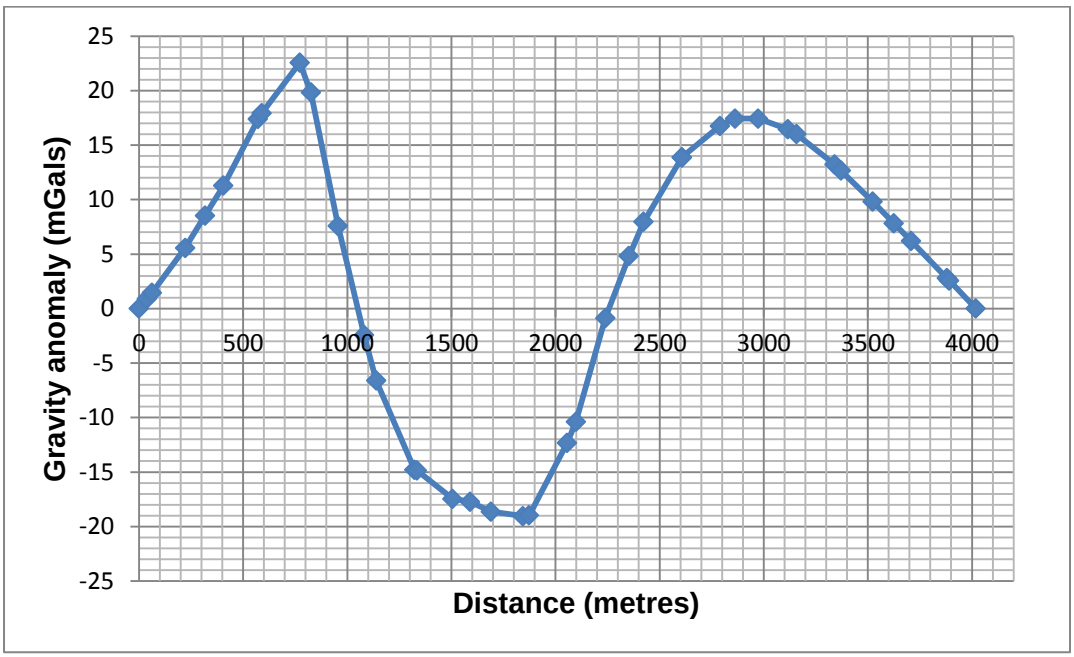

Figure 5.5 Profile BB' without regional trend

The gravity anomaly is observed to be rising to a maximum value at 800m along the profile. At 2800m along the profile is another maximum value of the gravity anomaly. The data from profile BB' was analyzed using Euler deconvolution. The figure 5.6 shows the results obtained from the Euler deconvolution. These results were used to discern fault lines, causative deep and shallow bodies along profile.

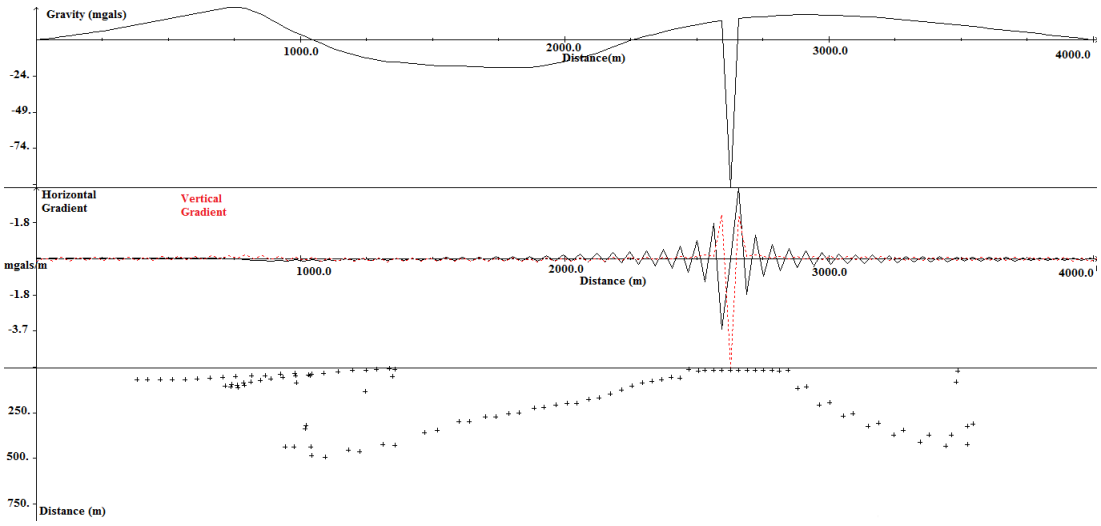

Figure 5.6 Euler deconvolution of profile BB' data

There are deep causative bodies at the various points along the profile. At between 1000m and 1250 m at a maximum depth of 600m and between 3250m and 3500m at a maximum depth of 500m were noted to have deep causative bodies. There is a wide shallow causative body at between 250m and 1250m at a maximum depth of 200m. Also between 2550 and 2900 is a shallow causative body, which is very close to the surface. There is only one major point of discontinuity along the profile. This suggests a Fault line at between 0m and 300m along the profile. Other discontinuities are very narrow and almost unnoticeable.

5.2.4 Gravity Profile CC'

The profile CC' as in figure 4.3 is about 14250m long and along the North - West direction. Using surfer software, the profile was digitized, sliced and data scattered to plot curves of the profile trend. The figure 5.7 shows the profile with regional trend.

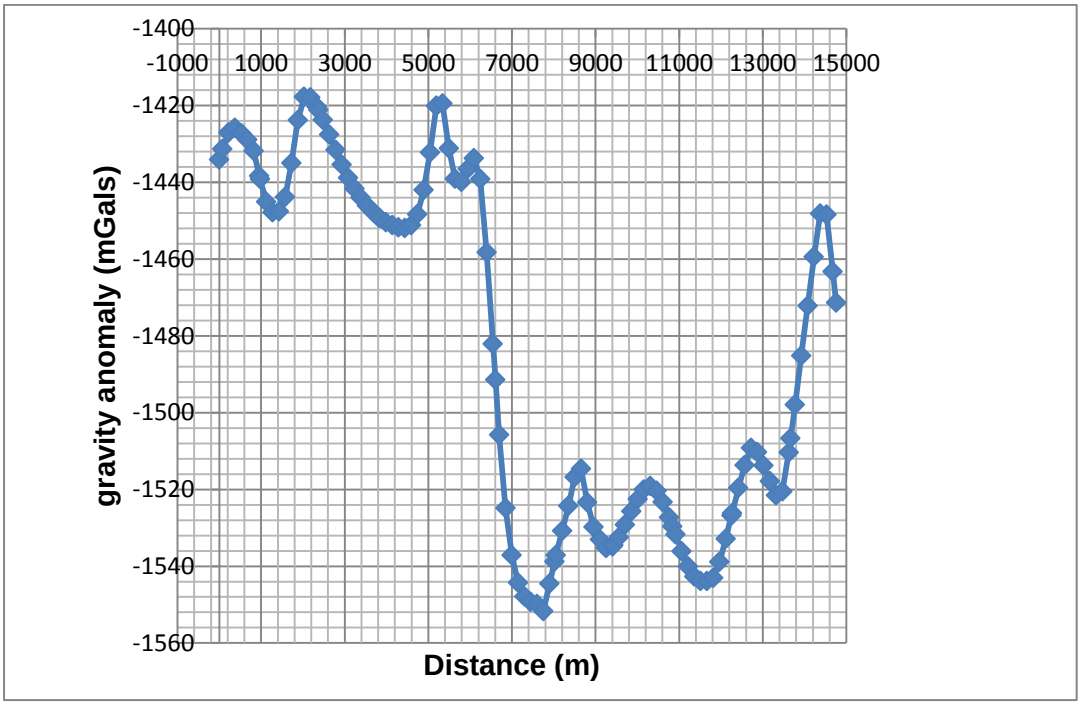

Figure 5.7 Profile CC' with regional trend

The regional trend was removed and figure 5.8 shows the profile without the regional trend.

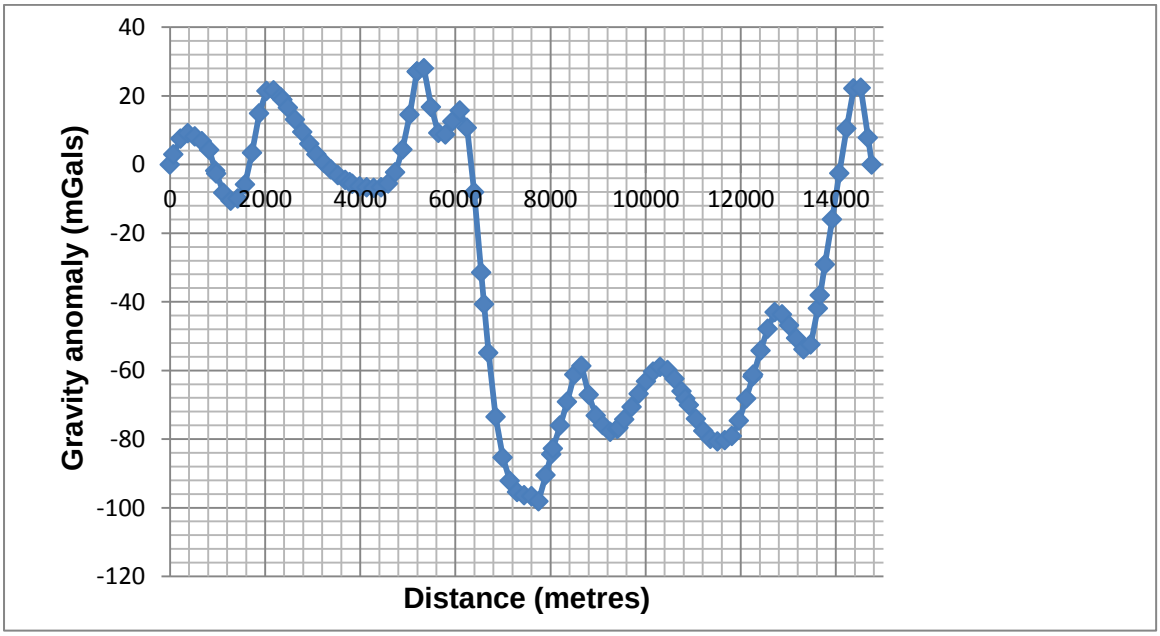

Figure 5.8 Profile CC' without regional trend

The gravity anomaly goes on varying along the profile. At 6000m, the anomaly drops to a minimum value along the profile. The data from profile CC' was analyzed using Euler deconvolution. The figure 5.9 shows the graph obtained from the Euler deconvolution. These results were used to discern fault lines, causative deep and shallow bodies along profile.

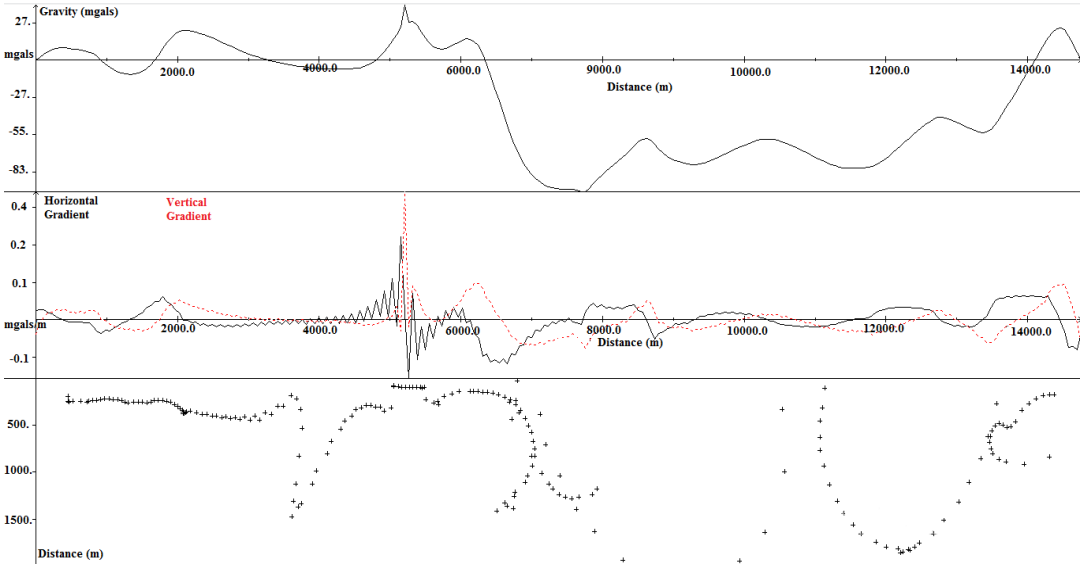

Figure 5.9 Euler deconvolution of profile CC' data

There is observed generally a shallow causative body along this profile at between 250m and 4000m at a depth of 400m. Also between 4250m and 6000m at a depth of 300m and at 14000m at a depth of 100m are observed to have shallow thermal bodies. The deepest causative body is at 4000m at a maximum depth of 1500m. Also at between 6250 and 8000m along the profile a maximum depth of 1500m is also observed. At 12000m along the profile at a maximum depth of 1800m was also seen to have a deep causative body. A major discontinuity (fault line) is observed to be between 0m and 250m. Discontinuities are also observed between 8000m and 9000m and between 1050m and 1100m along the profile.

5.3 Quantitative Analysis

The causative body of the gravity anomaly was simulated by a model whose theoretical anomaly could be computed. The shape of the model was altered until the computed anomaly closely matched the observed anomaly. Because of the inverse problem, this model could not be a unique interpretation, but ambiguity was

minimized by using other constraints on the nature and form of the anomalous body. A simple approach to this indirect interpretation was the comparison of the observed anomaly with the computed anomaly for certain standard geometrical shape whose size, position, form and density contrast are altered to improve the fit.

5.3.1 Model AA'

There is a continuous causative body of about 4000m long as shown in figure 5.10. The body protrudes up to a depth of 450m and has a density contrast of about 0.2634gcm^{-3}. The actual density is 2.9334gcm^{-3}, which is the density of a type of intrusive igneous rock. Just below the surface is a layer of sediments of thickness between 0m and 100m and of density contrast of -0.45gcm^{-3}. The actual density is 2.22gcm^{-3}, which is the average density of sediments.

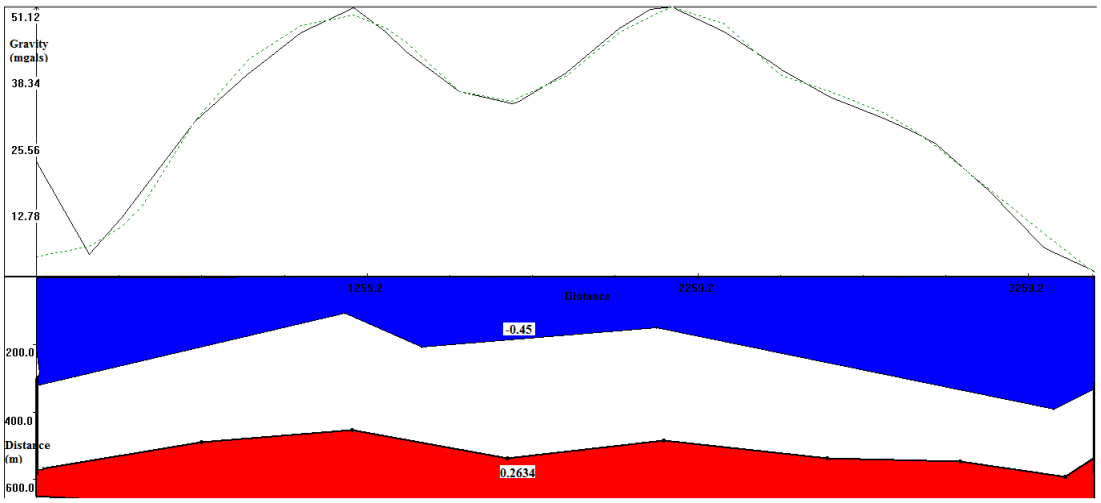

Figure 5.10 Model AA'

5.3.2 Model BB'

A causative body protrudes at 600m along the profile at a depth of 300m as shown in figure 5.11. At 3000m, it also protrudes up to a depth of 400m. At 1750m along the profile, the thermal body is at a depth of 800m below the surface. The causative body has a density contrast of 0.2475gcm^{-3}. The actual density is 2.9175gcm^{-3}, which is the density of a type of intrusive igneous rock. There is a layer of sedimentary rocks along the profile of up to a depth of 250m with a density contrast of 0.45gcm^{-3}.

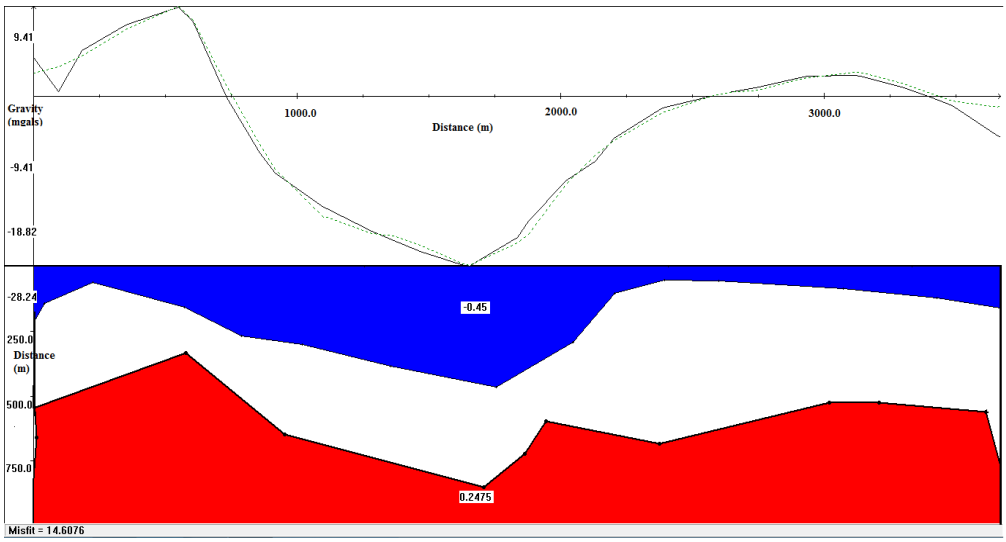

Figure 5.11 Model BB'

5.3.3 Model CC'

There is a causative body that protrudes between 0m and 600m along the profile at depth of 300m as shown in figure 5.12. At 7000m and 13000m along the profile, the causative body is at a depth of 700m. This causative body has a density contrast of 0.2850gcm^{-3}. The actual density of the rock is 2.955gcm^{-3}, which is the density of an intrusive igneous rock. There is a layer of sedimentary rocks along the profile of up to a depth of 200m of a density contrast of -0.45gcm^{-3}.

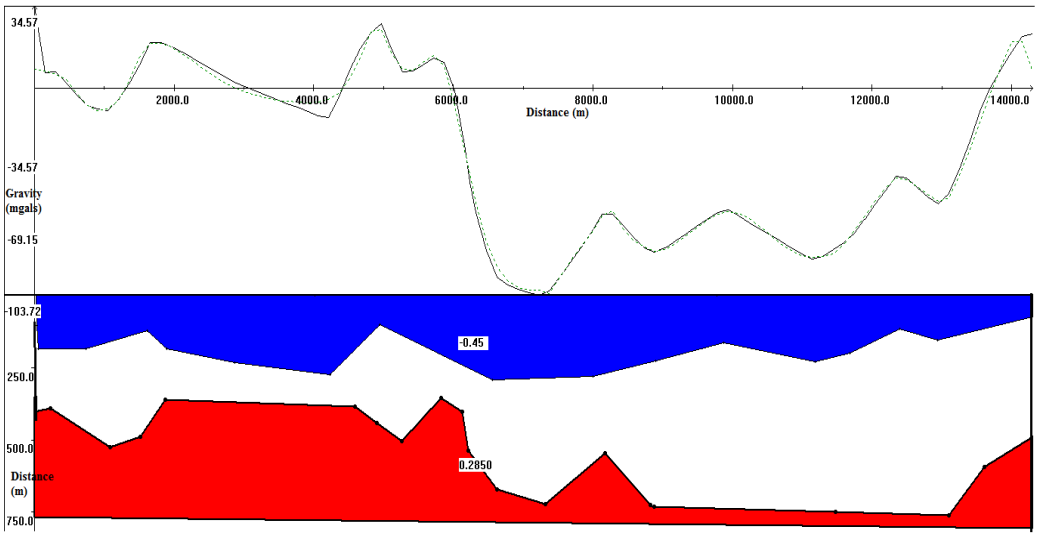

Figure 5.12 Model CC'

CHAPTER SIX

CONCLUSIONS AND RECOMENDATIONS

6.1 Conclusions

The primary goal of studying detailed gravity data is to provide a better understanding of the subsurface geology. The gravity survey from this area shows gravity highs ranging from between -1620 and -1400 mGals. This reveals the extent of gravity highs in the area. To further study the extent of the gravity high, the data was taken through qualitative and quantitative analysis. From the qualitative analysis, the gravity anomaly contour maps drawn reveal that the Northern and Southern sides of the area are gravity high zones while between the Northern and Southern are slightly low gravity highs. The Euler deconvolution on the profile data reveal that, there are faults/fractures or areas of discontinuity along the profiles. This may form conduits of geothermal fluid flow in Moinonin area of Lake Baringo. The conduits are very crucial in replenishing the geothermal system. These areas of discontinuity spread all along each profile. The Faults/fractures are known to lie in the relatively gravity high signature regions. Faults are also known to commonly juxtapose rocks of differing densities.

From the quantitative analysis models, the gravity survey conducted reveal possible heat sources in various regions of Moinonin area. These thermal bodies are the geothermal heat source and protrude up to a depth of between 300m and 750m below the surface. It also covered the all length of the profiles. These heat sources are probably due to intrusive dikes of high density along the gravity high areas caused by heavy rocks of high density. The density of the intrusive body range from 2.9175gcm^{-}

^{3} and 2.955gcm^{-3}. This is the average density of an intrusive igneous rock. The area is covered by sedimentary rock whose depth from the surface is 250m.

6.2 Recommendations

The recommendations from this research are geared towards establishing a heat reservoir in Moinonin area. It also aims at reducing the ambiguity associated with geothermal research. This will result in exploration of geothermal resource for production of electricity. Other methods of study can be used only to verify the findings of this study. The others include Thermal methods (soil temperature, heat flow), Electrical methods (resistivity, self-potential), Magnetic method (rock magnetization) and Seismic methods (wave velocity, seismicity, geological structures). There is no superior method and therefore integration of different geophysical techniques is effective in mapping defined structures in tectonic regimes where geothermal resources can be found. However, electrical and electromagnetic methods are commonly applied before geothermal exploration. Gravity method used at the study area thus has succeeded as a primary exploration tool. However, the interpretation of the gravity survey data is limited by ambiguity and the assumption of homogeneity. The ambiguity arises because an infinite number of possible sources could cause any given anomaly. For example, a distribution of small masses at a shallow depth can produce the same effect as a large mass at depth. The Gravity method also detected only lateral contrasts in density. There are other methods that can detect vertical, as well as lateral contrasts. These other methods therefore should be used to minimize the ambiguity and further determine the position of heat reservoir. The Combination of several methods will yield better interpretation. An assessment of the temperature of intrusion is required. The super-heated water now

needs to be identified and tapped for the generation of electricity. Direct utilization of geothermal energy also needs to be exploited. This includes its usage in domestic, horticulture, industry and fish farming among others.

REFERENCES

Baker, B.H., (1986). Tectonics and volcanism of the southern Kenya Rift valley and its influence on sedimentation in the African rifts.

Baker, B.H., Mohr, P.A. and Williams, L.A.J., (1972). Geology of the Eastern Rift System of Africa. *Special Paper* **136**: 1-67.

Baker, B. and Wohlenberg, J., (1971). "Structure and Evolution of the Kenya Rift Valley." *Nature* **229 (5286)**: 538–542.

Baker, B., Williams, L.A.J., Miller, J.A. and Fitch, F.J., (1971). "Sequence and Geochronology of the Kenya Rift Volcanics." *Tectonophysics* **11**: 191-215.

Black, S., Macdonald, R. and Kelly, M.R., (1997). Crustal origin for peralkaliner hyolites from Kenya: evidence from U-series Disequilibria and Th-Isotopes. *Journal of Petrology* **38:** 277–297.

Chapman, G., and Maureen B., (1978). "Chronostratigraphy of the Baringo Basin, Kenya." In Geological Background to Fossil Man. *Special Publication.* **6**: 207-223.

Dagley, P., Mussett, A. E. and Palmer, H. C., (1978). Preliminary observations on the palaeomagnetic stratigraphy of the area west of Lake Baringo, Kenya. *Geological society London Special Publication*. **6** (1): 225-235.

Dunkley, P. N., Smith, M., Allen D.J. and Darling, W.G. (1993): The geothermal activity and geology of the north sector of the Kenya Rift Valley. British Geological Survey, research report SC/93/1.

Karekezi, S. and Kithyoma, W., (2002). 'Renewable Energy Strategies for Rural Africa: is a PV Led Renewable Energy Strategy the Right approach for Providing Modern Energy to the Rural Poor of Sub-Saharan Africa? *Energy Policy* **30**: 11-12.

Karekezi, S. and Kimani, J., (2002). 'Status of Power Sector Reform on the Poor', *Energy Policy*, **30**:11-12, Special Issue – Africa: Improving Modern Energy Services for the Poor. Oxford: Elsevier Science Limited.

Kyalo, M. J., (2011). Integrated geophysical study of Lake Bogoria basin, Kenya: Implications for geothermal energy prospecting, PhD dissertation, University of Nairobi, Kenya.

Lagat, J., Mungania, J., and Opondo, K., (2005). Geoscientific Evaluation of the Lake Baringo Geothermal Prospect. KenGen Geothermal Resource Assessment Draft Report.

Lund, J.W., Freeston, D.H., and Boyd, T.L., (2005): Direct application of geothermal energy: 2005 worldwide review. *Geo-thermics* **34**: 691-727.

Macdonald, R., Davies, G. R., Bliss, C. M., Leat, P. T., Bailey, D. K. and Smith, R. L., (1987). Geochemistry of high-silica peralkaline rhyolites Naivasha, Kenya Rift Valley. *Journal of Petrology*, **28** part 6: 979-1008.

Marietta W. M., (2000): Stable Isotopic Composition of Geothermal Fields in Kenya; The Relationship between Geothermal Fields and Kenya Rift Lakes Waters.

Mariita, N.O., (1995). Exploration for Geothermal Energy in Kenya - a Historical Perspective. Kyushu University, Japan, Geothermal Research Report.

Mariita, N.O., (2003). An Integrated geophysical study of the northern Kenya rift crustal structure: Implications for geothermal energy prospecting for Menengai area. PhD dissertation, University of Texas at El Paso, USA. pp. 1-188.

Mariita, N.O. and Kilele, D.K., (1989). Geophysical report on Schlumberger survey: North of Lake Baringo. A Ministry of Energy, Government of Kenya report.

Martyn, J., (1969). The geologic history of the country between Lake Baringo and the Kerio River, Baringo District Kenya. Ph.D. Dissertation, University of London.

Mwangi, M. N, (2005) Country up date report for Kenya 2000-2005. Proceedings of the World Geothermal Congress 2005, Antalya, Turkey, CD, 10 pp.

Mwangi, M.N., (1984). A review of geophysical data of Olkaria geothermal field for STRM Nov. 1984.KPC/4P/OW/007.

Naomi, U., (1981). Crustal detachment during south atlantic rifting and formation of tucano – Gabon basin system. PHD dissertation, university of Durham, UK.

Ndombi, J.M., (1981). The Structure of the Shallow Crust beneath the Olkaria Geothermal field, Kenya, deduced from gravity studies. *Journal of Volcanic. Geothermal Resource.* **9**: 237-251.

Omenda, P.A., (2007). Status of Geothermal Exploration in Kenya and Future Plans for its development, KenGen special report, Naivasha, Kenya.

Omenda, PA., (1998). "The Geology and Structural Controls of the Olkaria Geothermal System, Kenya." *Geothermics* **27** (1): 55–74.

Simiyu, S.M., (2010). Status of Geothermal Exploration in Kenya and Future Plans for Its Development. World geothermal congress report in Bali Indonesia.

Simiyu, S.M. and Keller, G.R., (1997). Integrated geophysical analysis of the East African Plateau from gravity anomalies and recent seismic studies. *Tectonophysics* **278**: 291-314.

Stefansson, V., (1999). No success for renewables without geothermal energy. Paper presented at the European Geothermal Energy Council Seminar EGEC´99, April 29-30, Ferrara, Italy, 15pp.

Tallon P.W.J., 1978. Geological setting of the hominid fossils and Acheulian artifacts from the Kapthurin Formation, Baringo District, Kenya. In W.W. Bishop (Ed.), *Geological Background to Fossil Man* **10**: 257–277.

Truckle, P.H., (1977).Geological map of Lake Baringo Laikipia area, Directorate of overseas surveys, ordnance survey.

Woollard, G. P. and Rose J.C., (1980) International gravity measurements. A special publication for explorers and geophysicists, pp518.

APPENDIX I: Gravity station readings.

DAY	TIME	STATION NAME	EASTINGS	NORTHINGS	ELEVATION	STATION DIAL READING
DAY 1	10:20AM	KPS001	72555	167828	1024	623
	12:30pm	KPS002	72555	168028	1028	648
	3:00pm	KPS003	72555	165014	1015	608
	5:00pm	KPS004	72555	167616	1018	659
DAY 2	9:20am	KPS005	72555	168484	1016	608
	11:30am	KPS006	72555	165873	1042	647
	2:00pm	KPS007	72555	165561	1049	612
	3:30pm	KPS008	72555	166057	1075	643
	5:00pm	KPS009	72555	166412	1025	635
	6:30pm	KPS010	72555	166859	1018	628
DAY 3	9:00am	KPS011	72031	167818	1016	627
	11:30am	KPS012	72031	166901	1002	619
	2:30pm	KPS013	72031	168191	1056	628
	4:00pm	KPS014	72031	166541	1011	691
	5:20pm	KPS015	72031	166217	1034	616
DAY 4	9:30am	KPS016	72031	168512	1068	675
	10:20am	KPS017	72031	165702	1096	674
	2:00pm	KPS018	71204	167582	1022	676
	4:30pm	KPS019	71204	165918	1056	688
DAY 5	9:30am	KPS020	71204	167191	1049	648
	11:00am	KPS021	71204	167781	1028	658
	2:00pm	KPS022	71204	165344	1030	691
	3:30pm	KPS023	71204	168300	1036	668
DAY 6	9:00am	KPS024	71204	165011	1047	641
	10:30am	KPS025	71204	168104	1036	648
	1:00pm	KPS026	71204	166115	1031	696
	2:00pm	KPS027	71204	166897	1027	651
	4:00pm	KPS028	71204	166561	1011	688
DAY 7	9:00am	NG001	70418	165248	1038	656
	11:00am	NG002	70221	168856	1086	593
	2:00pm	NG003	70221	168615	1086	592
	4:20pm	NG004	70418	165637	1008	642
DAY 8	9:00am	NG005	70418	165983	1035	646
	10:00am	NG006	70418	166356	1202	519
	2:00pm	NG007	70221	168322	1012	625
	3:00pm	NG008	70418	166691	1021	612
	4:30pm	NG009	70418	167101	1026	661

DAY 9	9:00am	NG010	70221	167873	1033	643
	10:00am	NG011	70418	167465	1045	628
	2:00pm	MN001	73681	168030	1065	681
	3:00pm	MN002	73681	168659	1053	603
	4:30pm	MN003	73681	165231	1095	606
DAY 10	9:00am	MN004	73681	165639	1023	608
	11:00am	MN005	73681	166452	1047	661
	3:00pm	MN006	73681	166893	1031	622
	5:00pm	MN007	73681	167219	1026	628
DAY 11	9:00am	MN008	73681	167657	1053	621
	11:00am	MN009	74246	165830	1046	621
	2:00pm	MN010	74246	166336	1024	622
	4:00pm	MN011	74246	166859	1023	621
DAY 12	9:00am	MN012	74719	168691	1020	624
	11:00am	MN013	74246	165422	1053	624
	2:00pm	MN014	74719	168995	1060	624
	3:00pm	MN015	74246	165062	1058	624
	4:00pm	MN016	74246	167446	1012	619
DAY 13	9:00am	MN017	74719	168037	1031	615
	11:00am	KPU001	74246	167013	1017	613
	1:00pm	KPU002	75222	165002	1010	626
	2:00pm	KPU003	75222	167719	1011	624
	4:00pm	KPU004	75222	167988	1010	623
	6:00pm	KPU005	75222	165534	1010	628
DAY 14	9:00am	KPU006	75222	165999	1008	623
	11:00am	KPU007	75222	166371	1010	631
	2:00pm	KPU008	75222	168261	1017	627
	3:00pm	KPU009	75222	168669	1018	627
	5:00pm	KPU010	75222	166867	1030	623
DAY 15	8:45am	KPU011	76137	167421	1066	613
	11:00am	KPU012	76137	168701	1008	605
	2:15pm	KPU013	76137	168216	1033	607
	3:00pm	KPU014	76137	165032	1031	605
	5:20pm	KPU015	76137	165573	1038	609
DAY 16	9:00am	KPU016	76137	167781	1041	606
	10:30am	KPU017	76137	166058	1013	605
	1:00pm	KPU018	76137	166666	1000	607
	4:00pm	KPU019	76137	167043	1045	607
DAY 17	10:20AM	KPU020	76834	168038	1052	607
	12:30pm	KPU021	76834	168610	1068	610
	3:00pm	KPU022	76834	166507	1097	610

	5:00pm	KPU023	76834	166983	1086	611
DAY 18	9:00am	KPU024	77856	166878	1053	640
	11:00am	KPU025	77856	167428	1064	636
	3:00pm	KPU026	77856	167941	1015	638
	5:00pm	KPU027	77856	168758	1020	638
DAY 19	9:00am	KPU028	77856	168099	1013	628
	11:00am	KPU029	77856	166208	1037	634
	2:00pm	KPU030	77856	167792	1024	638
	4:00pm	KPU031	78213	167191	1019	660
	5:30pm	KPU032	78213	167691	1010	628
DAY 20	9:00am	KPU033	78213	168337	1009	634
	10:00pm	KPU034	78213	168832	1014	635
	2:00pm	CH001	69649	166304	1118	618
	4:00pm	CH002	69649	167442	1021	611
	5:00pm	CH003	69649	167816	1018	614
DAY 21	9:00am	CH004	69649	168243	1011	611
	10:30am	CH005	69112	166112	1120	607
	1:00pm	CH006	69112	167201	1012	605
	4:00pm	CH007	69112	167719	1000	603
DAY 22	9:20am	CH008	69112	168145	997	608
	11:30am	CH009	68715	166341	1017	609
	2:00pm	CH010	68715	167003	1012	609
	3:30pm	CH011	68715	167891	1000	610
	5:00pm	CH012	68715	168287	1000	607
	6:30pm	CH013	68271	166291	1014	605
DAY 23	9:30am	CH014	68271	166941	997	608
	11:00am	CH015	68271	167413	999	608
	2:00pm	CH016	67679	166703	1008	604
	3:30pm	KK001	67679	167112	994	595
DAY 24	9:00am	KK002	67679	167402	968	608
	11:00am	KK003	66561	166509	978	611
	2:00pm	KK004	66561	167231	982	609
	4:20pm	KK005	65419	166397	995	590
DAY 25	9:00am	KK006	65419	167021	982	540
	10:00am	KK007	65419	167419	1000	538
	2:00pm	KK008	65104	166041	998	590
	3:00pm	KK009	65104	166819	1001	586
	4:30pm	KK010	65104	167187	984	586
DAY 27	9:00am	KK011	65104	168314	980	533
	11:00am	KK012	64283	166319	1000	586
	2:00pm	KK013	64283	166891	998	545

	4:00pm	KK014	64283	167197	1001	584
DAY 28	9:00am	KK015	64283	167743	980	589
	11:00am	KK016	64283	168219	980	589
	1:00pm	KK017	63703	166421	1000	584
	2:00pm	KK018	63703	166980	1002	586
	4:00pm	KK019	63703	167313	987	585
	6:00pm	KK020	63703	167813	980	589
DAY 29	9:20am	KK021	63703	169304	972	583
	11:30am	KK022	63391	166119	980	592
	2:00pm	KK023	63391	166645	1000	587
	3:30pm	KK024	63391	167014	998	588
	5:00pm	KK025	63391	167639	960	584
	6:30pm	KK026	63391	168401	1002	588

APPENDIX II: Base station readings

	TIME	ELEVATION	EASTINGS	NORTHINGS	BASE STATION DIAL READING
	REFERENCE STATION	1017	73328	167549	602
DAY 1	8:30am	1018	72754	168114	620
	2:00pm	1018	72754	168114	650
	6:30pm	1018	72754	168114	610
DAY 2	8:00am	1016	73061	167818	598
	12:30pm	1016	73061	167818	629
	7:15pm	1016	73061	167818	595
DAY 3	8:00am	1032	73039	167212	618
	1:00pm	1032	73039	167212	611
	6:30pm	1032	73039	167212	621
DAY 4	8:00am	1043	71980	167570	684
	11:30am	1043	71980	167570	685
	3:00pm	1043	71980	167570	688
	6:30pm	1043	71980	167570	702
DAY 5	8:00am	1033	73027	167718	636
	12:00pm	1033	73027	167718	648
	5:30pm	1033	73027	167718	687
DAY 6	8:00am	1030	71880	167693	638
	12:00pm	1030	71880	167693	646
	3:00pm	1030	71880	167693	695
	6:00pm	1030	71880	167693	650
DAY 7	8:00am	1010	72755	168114	654
	12:00pm	1010	72755	168114	597
	5:00pm	1010	72755	168114	596
DAY 8	8:00am	1032	73061	167818	649
	12:00pm	1032	73061	167818	521
	6:00pm	1032	73061	167818	627
DAY 9	8:00am	1032	73320	167800	643
	1:00pm	1032	73320	167800	628
	6:30pm	1032	73320	167800	681
DAY 10	8:00am	1040	72988	167918	611
	12:30pm	1040	72988	167918	668
	6:00pm	1040	72988	167918	631
DAY 11	8:00am	1051	74672	166468	627
	12:00pm	1051	74672	166468	629
	5:30pm	1051	74672	166468	631
DAY 12	8:00am	1054	74680	168477	635

	12:30pm	1054	74680	168477	637
	6:00pm	1054	74680	168477	638
DAY 13	8:00am	1009	73972	167050	632
	12:00pm	1009	73972	167050	629
	3:00pm	1009	73972	167050	641
	7:00pm	1009	73972	167050	638
	8:00am	1011	74970	166994	633
DAY 14	1:00pm	1011	74970	166994	639
	6:00pm	1011	74970	166994	634
	8:20am	1017	74318	167100	615
DAY 15	12:45pm	1017	74318	167100	605
	6:30pm	1017	74318	167100	606
DAY 16	8:00am	1039	75316	167111	602
	12:00pm	1039	75316	167111	603
	6:00pm	1039	75316	167111	606
DAY 17	8:30am	1048	74580	167532	612
	2:00pm	1048	74580	167532	618
	6:30pm	1048	74580	167532	618
DAY 18	8:00am	1040	76586	167531	645
	12:00pm	1040	76586	167531	640
	6:00pm	1040	76586	167531	641
DAY 19	8:00am	1008	77280	168800	629
	12:00pm	1008	77280	168800	634
	3:00pm	1008	77280	168800	637
	7:00pm	1008	77280	168800	659
DAY 20	8:00am	1010	77684	168933	633
	12:00pm	1010	77684	168933	634
	6:00pm	1010	77684	168933	618
DAY 21	8:00am	1039	70590	167332	612
	12:00pm	1039	70590	167332	608
	6:00pm	1039	70590	167332	606
DAY 22	8:00AM	1016	70218	168356	605
	12:30PM	1016	70218	168356	607
	7:15PM	1016	70218	168356	607
DAY 23	8:00am	1033	70121	167800	608
	12:00pm	1033	70121	167800	608
	5:30pm	1033	70121	167800	605
DAY 24	8:00am	1010	68812	169217	609
	12:00pm	1010	68812	169217	612
	5:00pm	1010	68812	169217	610
DAY 25	8:00am	1032	66298	168504	540
	12:00pm	1032	66298	168504	538
	6:00pm	1032	66298	168504	593

DAY 26	8:00am	1014	65789	169521	535
	12:30pm	1014	65789	169521	588
	6:00pm	1014	65789	169521	547
DAY 27	8:00am	1000	66381	166537	590
	12:00pm	1000	66381	166537	590
	3:00pm	1000	66381	166537	584
	7:00pm	1000	66381	166537	586
DAY 28	8:00AM	1016	65164	169519	584
	12:30PM	1016	65164	169519	594
	7:15PM	1016	65164	169519	591
DAY 29	8:00AM	1016	65164	169519	584
	12:30PM	1016	65164	169519	594
	7:15PM	1016	65164	169519	591

APPENDIX III: Observed gravity

REF DIAL	STN DIAL	DRIFT	Crr stn dial reading	STN - REF	*0.10062	g_{abs}	g_{obs}
602	623	10	613	11	1.10682	977641	977642.41
602	648	20	628	26	2.61612	977641	977643.92
602	608	20	588	-14	-1.40868	977641	977639.89
602	659	5	654	52	5.23224	977641	977646.53
602	608	10	598	-4	-0.40248	977641	977640.90
602	647	25	622	20	2.0124	977641	977643.31
602	612	20	592	-10	-1.0062	977641	977640.29
602	643	15	628	26	2.61612	977641	977643.92
602	635	5	630	28	2.81736	977641	977644.12
602	628	-5	633	31	3.11922	977641	977644.42
602	627	-5	632	30	3.0186	977641	977644.32
602	619	-5	624	22	2.21364	977641	977643.51
602	628	-5	633	31	3.11922	977641	977644.42
602	691	1	690	88	8.85456	977641	977650.15
602	616	4	612	10	1.0062	977641	977642.31
602	675	10	665	63	6.33906	977641	977647.64
602	674	4	670	68	6.84216	977641	977648.14
602	676	8	668	66	6.64092	977641	977647.94
602	688	30	658	56	5.63472	977641	977646.93
602	648	44	604	2	0.20124	977641	977641.50
602	658	2	656	54	5.43348	977641	977646.73
602	691	5	686	84	8.45208	977641	977649.75
602	668	22	646	44	4.42728	977641	977645.73
602	641	34	607	5	0.5031	977641	977641.80
602	648	-15	663	61	6.13782	977641	977647.44
602	696	-40	736	134	13.48308	977641	977654.78
602	651	-55	706	104	10.46448	977641	977651.76
602	688	-60	748	146	14.69052	977641	977655.99
602	656	-35	691	89	8.95518	977641	977650.26
602	593	-65	658	56	5.63472	977641	977646.93
602	592	-90	682	80	8.0496	977641	977649.35
602	642	-75	717	115	11.5713	977641	977652.87
602	646	-45	691	89	8.95518	977641	977650.26
602	519	-5	524	-78	-7.84836	977641	977633.45
602	625	-5	630	28	2.81736	977641	977644.12
602	612	-5	617	15	1.5093	977641	977642.81
602	661	5	656	54	5.43348	977641	977646.73

602	643	15	628	26	2.61612	977641	977643.92
602	628	12	616	14	1.40868	977641	977642.71
602	681	36	645	43	4.32666	977641	977645.63
602	603	38	565	-37	-3.72294	977641	977637.58
602	606	24	582	-20	-2.0124	977641	977639.29
602	608	1	607	5	0.5031	977641	977641.80
602	661	3.5	657.5	55.5	5.58441	977641	977646.88
602	622	5	617	15	1.5093	977641	977642.81
602	628	5.5	622.5	20.5	2.06271	977641	977643.36
602	621	1	620	18	1.81116	977641	977643.11
602	621	2	619	17	1.71054	977641	977643.01
602	622	2	620	18	1.81116	977641	977643.11
602	621	2	619	17	1.71054	977641	977643.01
602	624	-1	625	23	2.31426	977641	977643.61
602	624	-2	626	24	2.41488	977641	977643.71
602	624	1	623	21	2.11302	977641	977643.41
602	624	5	619	17	1.71054	977641	977643.01
602	619	8	611	9	0.90558	977641	977642.21
602	615	6.5	608.5	6.5	0.65403	977641	977641.95
602	613	1	612	10	1.0062	977641	977642.31
602	626	3.5	622.5	20.5	2.06271	977641	977643.36
602	624	5	619	17	1.71054	977641	977643.01
602	623	4	619	17	1.71054	977641	977643.01
602	628	-10	638.2	36.2	3.642444	977641	977644.94
602	623	-6	629	27	2.71674	977641	977644.02
602	631	-10	641	39	3.92418	977641	977645.22
602	627	0.5	626.5	24.5	2.46519	977641	977643.77
602	627	0.7	626.3	24.3	2.445066	977641	977643.75
602	623	1.3	621.7	19.7	1.982214	977641	977643.28
602	613	3	610	8	0.80496	977641	977642.10
602	605	4.4	600.6	-1.4	-0.140868	977641	977641.16
602	607	4.6	602.4	0.4	0.040248	977641	977641.34
602	605	6	599	-3	-0.30186	977641	977641.00
602	609	6	603	1	0.10062	977641	977641.40
602	606	-1.3	607.3	5.3	0.533286	977641	977641.83
602	605	-3.8	608.8	6.8	0.684216	977641	977641.98
602	607	-4.5	611.5	9.5	0.95589	977641	977642.26
602	607	-4.2	611.2	9.2	0.925704	977641	977642.23
602	607	5	602	0	0	977641	977641.30
602	610	5	605	3	0.30186	977641	977641.60
602	610	10	600	-2	-0.20124	977641	977641.10

602	611	20	591	-11	-1.10682	977641	977640.19
602	640	0	640	38	3.82356	977641	977645.12
602	636	2	634	32	3.21984	977641	977644.52
602	638	5	633	31	3.11922	977641	977644.42
602	638	10	628	26	2.61612	977641	977643.92
602	628	12	616	14	1.40868	977641	977642.71
602	634	-1	635	33	3.32046	977641	977644.62
602	638	-2.5	640.5	38.5	3.87387	977641	977645.17
602	660	-4.5	664.5	62.5	6.28875	977641	977647.59
602	628	0.5	627.5	25.5	2.56581	977641	977643.87
602	634	1.5	632.5	30.5	3.06891	977641	977644.37
602	635	2	633	31	3.11922	977641	977644.42
602	618	0	618	16	1.60992	977641	977642.91
602	611	0	611	9	0.90558	977641	977642.21
602	614	1	613	11	1.10682	977641	977642.41
602	611	2	609	7	0.70434	977641	977642.00
602	607	0.5	606.5	4.5	0.45279	977641	977641.75
602	605	2	603	1	0.10062	977641	977641.40
602	603	2	601	-1	-0.10062	977641	977641.20
602	608	1.5	606.5	4.5	0.45279	977641	977641.75
602	609	0	609	7	0.70434	977641	977642.00
602	609	0	609	7	0.70434	977641	977642.00
602	610	15	595	-7	-0.70434	977641	977640.60
602	607	25	582	-20	-2.0124	977641	977639.29
602	605	35	570	-32	-3.21984	977641	977638.08
602	608	15	593	-9	-0.90558	977641	977640.39
602	608	40	568	-34	-3.42108	977641	977637.88
602	604	45	559	-43	-4.32666	977641	977636.97
602	595	30	565	-37	-3.72294	977641	977637.58
602	608	0	608	6	0.60372	977641	977641.90
602	611	0	611	9	0.90558	977641	977642.21
602	609	-5	614	12	1.20744	977641	977642.51
602	590	-10	600	-2	-0.20124	977641	977641.10
602	540	-15	555	-47	-4.72914	977641	977636.57
602	538	-10	548	-54	-5.43348	977641	977635.87
602	590	3	587	-15	-1.5093	977641	977639.79
602	586	8	578	-24	-2.41488	977641	977638.89
602	586	10	576	-26	-2.61612	977641	977638.68
602	533	9	524	-78	-7.84836	977641	977633.45
602	586	8	578	-24	-2.41488	977641	977638.89
602	545	7	538	-64	-6.43968	977641	977634.86

602	584	-1.2	585.2	-16.8	-1.690416	977641	977639.61
602	589	-0.6	589.6	-12.4	-1.247688	977641	977640.05
602	589	-0.4	589.4	-12.6	-1.267812	977641	977640.03
602	584	-0.2	584.2	-17.8	-1.791036	977641	977639.51
602	586	0.2	585.8	-16.2	-1.630044	977641	977639.67
602	585	0.7	584.3	-17.7	-1.780974	977641	977639.52
602	589	-0.5	589.5	-12.5	-1.25775	977641	977640.04
602	583	-1.4	584.4	-17.6	-1.770912	977641	977639.53
602	592	-2	594	-8	-0.80496	977641	977640.50
602	587	-3.6	590.6	-11.4	-1.147068	977641	977640.15
602	588	-4.5	592.5	-9.5	-0.95589	977641	977640.34
602	584	-5.3	589.3	-12.7	-1.277874	977641	977640.02
602	588	-6	594	-8	-0.80496	977641	977640.50

APPENDIX IV: Complete Bouguer Anomaly (CBA)

GRAVITY STATION NAME	NORTHING	EASTING	ELEV (m)	g_{obs} (mGAL)	g_n (mGAL)	g_{fa} 0.3086h	gb 0.04193ρh	TC	CBA (mGAL)
KPS001	72555	167828	1024	977642.41	-979956.55	316.01	-114.64	0.1941	-1542.62
KPS002	72555	168028	1028	977642.41	-979956.55	317.24	-115.09	0.1553	-1516.81
KPS003	72555	165014	1015	977642.41	-979956.55	313.23	-113.63	0.2985	-1559.18
KPS004	72555	167616	1018	977642.41	-979956.55	314.15	-113.97	0.2611	-1507.71
KPS005	72555	168484	1016	977642.41	-979956.55	313.54	-113.74	0.2858	-1558.71
KPS006	72555	165873	1042	977642.41	-979956.55	321.56	-116.66	0.0559	-1514.86
KPS007	72555	165561	1049	977642.41	-979956.55	323.72	-117.44	0.0278	-1558.15
KPS008	72555	166057	1075	977642.41	-979956.55	331.75	-120.35	0.0493	-1512.33
KPS009	72555	166412	1025	977642.41	-979956.55	316.32	-114.75	0.1840	-1530.13
KPS010	72555	166859	1018	977642.41	-979956.55	314.15	-113.97	0.2611	-1539.08
KPS011	72031	167818	1016	977642.41	-979932.94	313.54	-113.74	0.2858	-1516.39
KPS012	72031	166901	1002	977642.41	-979932.94	309.22	-112.18	0.4904	-1527.23
KPS013	72031	168191	1056	977642.41	-979932.94	325.88	-118.22	0.0140	-1506.97
KPS014	72031	166541	1011	977642.41	-979932.94	311.99	-113.18	0.3524	-1553.19
KPS015	72031	166217	1034	977642.41	-979932.94	319.09	-115.76	0.1057	-1523.94
KPS016	72031	168512	1068	977642.41	-979932.94	329.58	-119.57	0.0239	-1558.04
KPS017	72031	165702	1096	977642.41	-979932.94	338.23	-122.70	0.2114	-1553.62
KPS018	71204	167582	1022	977642.41	-979895.51	315.39	-114.42	0.2471	-1528.77
KPS019	71204	165918	1056	977642.41	-979895.51	325.88	-118.22	0.2193	-1510.70
KPS020	71204	167191	1049	977642.41	-979895.51	323.72	-117.44	0.1975	-1551.69
KPS021	71204	167781	1028	977642.41	-979895.51	317.24	-115.09	0.2176	-1545.86
KPS022	71204	165344	1030	977642.41	-979895.51	317.86	-115.31	0.2101	-1512.69
KPS023	71204	168300	1036	977642.41	-979895.51	319.71	-115.98	0.1947	-1534.11
KPS024	71204	165011	1047	977642.41	-979895.51	323.10	-117.21	0.1938	-1558.47
KPS025	71204	168104	1036	977642.41	-979895.51	319.71	-115.98	0.1947	-1553.81
KPS026	71204	166115	1031	977642.41	-979895.51	318.17	-115.42	0.2068	-1507.03
KPS027	71204	166897	1027	977642.41	-979895.51	316.93	-114.98	0.2218	-1552.57
KPS028	71204	166561	1011	977642.41	-979895.51	311.99	-113.18	0.3284	-1518.76
NG001	70418	165248	1038	977642.41	-979860.37	320.33	-116.21	0.1919	-1510.23
NG002	70221	168856	1086	977642.41	-979851.86	335.14	-121.58	0.4725	-1557.04
NG003	70221	168615	1086	977642.41	-979851.86	335.14	-121.58	0.4725	-1557.88
NG004	70418	165637	1008	977642.41	-979860.37	311.07	-112.85	0.3568	-1530.36
NG005	70418	165983	1035	977642.41	-979860.37	319.40	-115.87	0.1966	-1521.58
NG006	70418	166356	1202	977642.41	-979860.37	370.94	-134.57	3.6968	-1619.42
NG007	70221	168322	1012	977642.41	-979851.86	312.30	-113.30	0.3196	-1538.11

NG008	70418	166691	1021	977642.41	-979860.37	315.08	-114.30	0.2530	-1557.97
NG009	70418	167101	1026	977642.41	-979860.37	316.62	-114.86	0.2263	-1508.16
NG010	70221	167873	1033	977642.41	-979851.86	318.78	-115.65	0.2011	-1516.37
NG011	70418	167465	1045	977642.41	-979860.37	322.49	-116.99	0.1914	-1537.65
MN001	73681	168030	1065	977642.41	-980007.72	328.66	-119.23	0.0175	-1527.12
MN002	73681	168659	1053	977642.41	-980007.72	324.96	-117.89	0.0181	-1508.07
MN003	73681	165231	1095	977642.41	-980007.72	337.92	-122.59	0.2007	-1557.03
MN004	73681	165639	1023	977642.41	-980007.72	315.70	-114.53	0.2046	-1549.39
MN005	73681	166452	1047	977642.41	-980007.72	323.10	-117.21	0.0343	-1550.70
MN006	73681	166893	1031	977642.41	-980007.72	318.17	-115.42	0.1292	-1513.59
MN007	73681	167219	1026	977642.41	-980007.72	316.62	-114.86	0.1741	-1508.20
MN008	73681	167657	1053	977642.41	-980007.72	324.96	-117.89	0.0181	-1518.29
MN009	74246	165830	1046	977642.41	-980033.47	322.80	-117.10	0.0224	-1542.88
MN010	74246	166336	1024	977642.41	-980033.47	316.01	-114.64	0.0810	-1531.02
MN011	74246	166859	1023	977642.41	-980033.47	315.70	-114.53	0.0870	-1542.83
MN012	74719	168691	1020	977642.41	-980055.10	314.77	-114.19	0.1069	-1540.74
MN013	74246	165422	1053	977642.41	-980033.47	324.96	-117.89	0.0337	-1512.80
MN014	74719	168995	1060	977642.41	-980055.10	327.12	-118.67	0.0593	-1532.48
MN015	74246	165062	1058	977642.41	-980033.47	326.50	-118.45	0.0505	-1512.05
MN016	74246	167446	1012	977642.41	-980033.47	312.30	-113.30	0.1727	-1526.12
MN017	74719	168037	1031	977642.41	-980055.10	318.17	-115.42	0.0469	-1547.69
KPU001	74246	167013	1017	977642.41	-980033.47	313.85	-113.86	0.1294	-1550.36
KPU002	75222	165002	1010	977642.41	-980078.18	311.69	-113.07	0.1921	-1533.56
KPU003	75222	167719	1011	977642.41	-980078.18	311.99	-113.18	0.1823	-1546.00
KPU004	75222	167988	1010	977642.41	-980078.18	311.69	-113.07	0.1921	-1556.50
KPU005	75222	165534	1010	977642.41	-980078.18	311.69	-113.07	0.1921	-1552.12
KPU006	75222	165999	1008	977642.41	-980078.18	311.07	-112.85	0.2127	-1546.91
KPU007	75222	166371	1010	977642.41	-980078.18	311.69	-113.07	0.1921	-1539.31
KPU008	75222	168261	1017	977642.41	-980078.18	313.85	-113.86	0.1294	-1531.06
KPU009	75222	168669	1018	977642.41	-980078.18	314.15	-113.97	0.1216	-1550.99
KPU010	75222	166867	1030	977642.41	-980078.18	317.86	-115.31	0.0509	-1532.69
KPU011	76137	167421	1066	977642.41	-980120.21	328.97	-119.34	0.3315	-1507.62
KPU012	76137	168701	1008	977642.41	-980120.21	311.07	-112.85	0.0560	-1506.95
KPU013	76137	168216	1033	977642.41	-980120.21	318.78	-115.65	0.0540	-1510.44
KPU014	76137	165032	1031	977642.41	-980120.21	318.17	-115.42	0.0474	-1512.89
KPU015	76137	165573	1038	977642.41	-980120.21	320.33	-116.21	0.0756	-1556.97
KPU016	76137	167781	1041	977642.41	-980120.21	321.25	-116.54	0.0921	-1509.87
KPU017	76137	166058	1013	977642.41	-980120.21	312.61	-113.41	0.0409	-1525.91
KPU018	76137	166666	1000	977642.41	-980120.21	308.60	-111.95	0.0954	-1507.30
KPU019	76137	167043	1045	977642.41	-980120.21	322.49	-116.99	0.1182	-1558.35
KPU020	76834	168038	1052	977642.41	-980152.13	324.65	-117.77	0.1751	-1518.50

KPU021	76834	168610	1068	977642.41	-980152.13	329.58	-119.57	0.3584	-1527.51
KPU022	76834	166507	1097	977642.41	-980152.13	338.53	-122.81	0.8764	-1537.11
KPU023	76834	166983	1086	977642.41	-980152.13	335.14	-121.58	0.6522	-1557.75
KPU024	77856	166878	1053	977642.41	-980199.35	324.96	-117.89	0.1844	-1520.93
KPU025	77856	167428	1064	977642.41	-980199.35	328.35	-119.12	0.3057	-1555.09
KPU026	77856	167941	1015	977642.41	-980199.35	313.23	-113.63	0.0369	-1543.86
KPU027	77856	168758	1020	977642.41	-980199.35	314.77	-114.19	0.0321	-1438.24
KPU028	77856	168099	1013	977642.41	-980199.35	312.61	-113.41	0.0409	-1471.99
KPU029	77856	166208	1037	977642.41	-980199.35	320.02	-116.10	0.0707	-1461.19
KPU030	77856	167792	1024	977642.41	-980199.35	316.01	-114.64	0.0335	-1470.16
KPU031	78213	167191	1019	977642.41	-980215.88	314.46	-114.08	0.0952	-1464.88
KPU032	78213	167691	1010	977642.41	-980215.88	311.69	-113.07	0.0969	-1509.76
KPU033	78213	168337	1009	977642.41	-980215.88	311.38	-112.96	0.0985	-1472.62
KPU034	78213	168832	1014	977642.41	-980215.88	312.92	-113.52	0.0932	-1480.98
CH001	69649	166304	1118	977642.41	-979825.94	345.01	-125.16	2.1151	-1410.73
CH002	69649	167442	1021	977642.41	-979825.94	315.08	-114.30	0.2240	-1442.59
CH003	69649	167816	1018	977642.41	-979825.94	314.15	-113.97	0.2070	-1431.73
CH004	69649	168243	1011	977642.41	-979825.94	311.99	-113.18	0.1774	-1440.71
CH005	69112	166112	1120	977642.41	-979802.42	345.63	-125.39	2.1798	-1437.37
CH006	69112	167201	1012	977642.41	-979802.42	312.30	-113.30	0.1808	-1480.25
CH007	69112	167719	1000	977642.41	-979802.42	308.60	-111.95	0.1598	-1443.09
CH008	69112	168145	997	977642.41	-979802.42	307.67	-111.62	0.1612	-1451.46
CH009	68715	166341	1017	977642.41	-979784.42	313.85	-113.86	0.2019	-1420.55
CH010	68715	167003	1012	977642.41	-979784.42	312.30	-113.30	0.1808	-1423.18
CH011	68715	167891	1000	977642.41	-979784.42	308.60	-111.95	0.1598	-1409.79
CH012	68715	168287	1000	977642.41	-979784.42	308.60	-111.95	0.1598	-1460.67
CH013	68271	166291	1014	977642.41	-979764.84	312.92	-113.52	0.1883	-1460.35
CH014	68271	166941	997	977642.41	-979764.84	307.67	-111.62	0.1612	-1416.38
CH015	68271	167413	999	977642.41	-979764.84	308.29	-111.84	0.1600	-1460.39
CH016	67679	166703	1008	977642.41	-979739.49	311.07	-112.85	0.1922	-1429.16
KK001	67679	167112	994	977642.41	-979739.49	306.75	-111.28	0.1635	-1460.50
KK002	67679	167402	968	977642.41	-979739.49	298.72	-108.37	0.2627	-1451.96
KK003	66561	166509	978	977642.41	-979926.70	301.81	-109.49	0.2010	-1453.22
KK004	66561	167231	982	977642.41	-979926.70	303.05	-109.94	0.1846	-1445.01
KK005	65419	166397	995	977642.41	-979640.55	307.06	-111.39	0.1525	-1455.96
KK006	65419	167021	982	977642.41	-979640.55	303.05	-109.94	0.2542	-1418.57
KK007	65419	167419	1000	977642.41	-979640.55	308.60	-111.95	0.1266	-1417.60
KK008	65104	166041	998	977642.41	-979626.32	307.98	-111.73	0.1361	-1441.21
KK009	65104	166819	1001	977642.41	-979626.32	308.91	-112.07	0.1223	-1454.23
KK010	65104	167187	984	977642.41	-979626.32	303.66	-110.16	0.2353	-1458.01
KK011	65104	168314	980	977642.41	-979626.32	302.43	-109.71	0.2742	-1412.09

KK012	64283	166319	1000	977642.41	-979590.83	308.60	-111.95	0.1266	-1409.02
KK013	64283	166891	998	977642.41	-979590.83	307.98	-111.73	0.1361	-1460.71
KK014	64283	167197	1001	977642.41	-979590.83	308.91	-112.07	0.1223	-1420.87
KK015	64283	167743	980	977642.41	-979590.83	302.43	-109.71	0.2742	-1460.75
KK016	64283	168219	980	977642.41	-979590.83	302.43	-109.71	0.2742	-1460.96
KK017	63703	166421	1000	977642.41	-979566.07	308.60	-111.95	0.1266	-1436.94
KK018	63703	166980	1002	977642.41	-979566.07	309.22	-112.18	0.1183	-1414.22
KK019	63703	167313	987	977642.41	-979566.07	304.59	-110.50	0.2092	-1427.95
KK020	63703	167813	980	977642.41	-979566.07	302.43	-109.71	0.2742	-1416.02
KK021	63703	169304	972	977642.41	-979566.07	299.96	-108.82	0.3660	-1443.49
KK022	63391	166119	980	977642.41	-979552.69	302.43	-109.71	0.2742	-1449.09
KK023	63391	166645	1000	977642.41	-979552.69	308.60	-111.95	0.1266	-1460.02
KK024	63391	167014	998	977642.41	-979552.69	307.98	-111.73	0.1361	-1439.56
KK025	63391	167639	960	977642.41	-979552.69	296.26	-107.47	0.5385	-1441.83
KK026	63391	168401	1002	977642.41	-979552.69	309.22	-112.18	0.1183	-1409.04

APPENDIX V: Profile data

Profile data AA' with regional trend

0	-1456.01
99.19822	-1455.77
116.1842	-1455.82
259.2044	-1455.4
419.2106	-1455.55
515.6792	-1453.02
579.2167	-1449.74
739.2229	-1435.41
899.2291	-1425.85
915.1743	-1425.24
1059.235	-1421.23
1219.241	-1421.22
1314.669	-1424.96
1379.248	-1428.52
1539.254	-1440.02
1699.26	-1443.91
1714.164	-1443.56
1859.266	-1441.14
2019.272	-1434.89
2113.659	-1433.05
2179.278	-1431.97
2339.285	-1437.2
2499.291	-1448.64
2513.155	-1449.36
2659.297	-1454.28
2819.303	-1460.44
2912.65	-1465.08
2979.309	-1468.91
3139.315	-1479.2
3299.322	-1489.51
3312.145	-1490.23
3459.328	-1499.43
3478.401	-1500.41

Profile data AA' without regional trend

0	-0.00455
99.19822	1.507355
116.1842	1.668076
259.2044	3.918696
419.2106	5.806972
515.6792	9.572386
579.2167	13.66037
739.2229	30.03489
899.2291	41.63595
915.1743	42.45585
1059.235	48.29565
1219.241	50.35658
1314.669	47.82645
1379.248	45.09935
1539.254	35.63814
1699.26	33.79147
1714.164	34.32562
1859.266	38.6058
2019.272	46.8984
2113.659	49.93613
2179.278	51.85379
2339.285	48.67097
2499.291	39.27046
2513.155	38.72447
2659.297	35.66959
2819.303	31.55807
2912.65	28.10757
2979.309	25.12812
3139.315	16.88368
3299.322	8.614571
3312.145	8.054436
3459.328	0.736442
3478.401	-0.00137

Profile BB' with regional trend

0	-1434.82
38.48707	-1433.94
62.76205	-1433.36
221.9442	-1429.26
317.2323	-1426.3
405.4014	-1423.55
571.7025	-1417.46
588.8585	-1416.92
772.3157	-1412.29
826.1728	-1415.02
955.7728	-1427.27
1080.643	-1437.27
1139.23	-1441.46
1322.687	-1449.67
1335.113	-1449.73
1506.144	-1452.32
1589.583	-1452.6
1689.601	-1453.5
1844.054	-1453.92
1873.059	-1453.85
2056.516	-1447.2
2098.524	-1445.27
2239.973	-1435.76
2352.994	-1430.08
2423.43	-1426.94
2606.887	-1421.04
2607.464	-1421.03
2790.344	-1418.15
2861.935	-1417.47
2973.801	-1417.48
3116.405	-1418.47
3157.259	-1418.91
3340.716	-1421.71
3370.875	-1422.26
3524.173	-1425.12
3625.345	-1427.11
3707.63	-1428.73
3879.816	-1432.14
3891.087	-1432.37
4019.122	-1434.94

Profile BB' without regional trend

0	0.001159
38.48707	0.884849
62.76205	1.460169
221.9442	5.568228
317.2323	8.52824
405.4014	11.28153
571.7025	17.37989
588.8585	17.91331
772.3157	22.55555
826.1728	19.8224
955.7728	7.581484
1080.643	-2.41706
1139.23	-6.61075
1322.687	-14.8063

1335.113	-14.8655
1506.144	-17.4583
1589.583	-17.7292
1689.601	-18.6324
1844.054	-19.0426
1873.059	-18.9773
2056.516	-12.3221
2098.524	-10.3835
2239.973	-0.87194
2352.994	4.814354
2423.43	7.953802
2606.887	13.85582
2607.464	13.8726
2790.344	16.75384
2861.935	17.4358
2973.801	17.42883
3116.405	16.44662
3157.259	16.00122
3340.716	13.21434
3370.875	12.66085
3524.173	9.807263
3625.345	7.816125
3707.63	6.205191
3879.816	2.79169
3891.087	2.570458
4019.122	0.001007

Profile CC' with regional trend

0	-1434.09
71.36199	-1431.34
221.9122	-1427.07
372.4623	-1425.86
523.0125	-1427.26
673.5626	-1428.97
824.1128	-1431.87
956.3735	-1438.33
974.6629	-1439.18
1125.213	-1445.11
1275.763	-1447.82
1426.313	-1447.62
1576.864	-1443.83
1727.414	-1435.01
1877.964	-1423.88
2028.514	-1417.77
2179.064	-1417.96
2329.614	-1420.31
2368.525	-1421.19
2480.164	-1423.73
2630.715	-1427.63

2781.265	-1431.64
2931.815	-1435.48
3082.365	-1438.88
3232.915	-1441.71
3383.465	-1444.07
3534.016	-1446.1
3684.566	-1447.88
3780.677	-1448.82
3835.116	-1449.36
3985.666	-1450.47
4136.216	-1451.22
4286.766	-1451.76
4437.317	-1451.98
4587.867	-1451.21
4738.417	-1448.34
4888.967	-1442.05
5039.517	-1432.27
5190.067	-1420.15
5192.828	-1420.11
5340.617	-1419.5
5491.168	-1431.23
5641.718	-1439.14
5792.268	-1439.97
5942.818	-1436.52
6093.368	-1433.75
6243.918	-1439.16
6394.469	-1458.28
6545.019	-1482.11
6604.98	-1491.48
6695.569	-1505.82
6846.119	-1524.87
6996.669	-1537.16
7147.219	-1544.35
7297.769	-1547.91
7448.32	-1549.3
7598.87	-1549.95
7749.42	-1551.79
7899.97	-1544.56
8017.132	-1538.79
8050.52	-1537.16
8201.07	-1530.85
8351.621	-1524.31
8502.171	-1516.8
8652.721	-1514.65
8803.271	-1523.44
8953.821	-1529.81
9104.371	-1533.06
9254.921	-1535.32
9405.472	-1534.92
9429.283	-1534.56
9556.022	-1532.52
9706.572	-1529.21
9857.122	-1525.74
10007.67	-1522.55
10158.22	-1520.09
10308.77	-1519.13
10459.32	-1520.36
10609.87	-1523.34
10760.42	-1527.31
10841.43	-1529.68
10910.97	-1531.72

11061.52	-1536.13
11212.07	-1540.05
11362.62	-1542.77
11513.17	-1543.87
11663.72	-1543.89
11814.27	-1543.06
11964.82	-1538.93
12115.37	-1532.87
12253.59	-1526.81
12265.92	-1526.26
12416.47	-1519.68
12567.02	-1513.7
12717.58	-1509.27
12868.13	-1510.31
13018.68	-1513.84
13169.23	-1517.93
13319.78	-1521.6
13470.33	-1520.54
13620.88	-1510.37
13665.74	-1506.69
13771.43	-1498.01
13921.98	-1485.18
14072.53	-1472.2
14223.08	-1459.46
14373.63	-1448.22
14524.18	-1448.44

Profile CC' without regional rend

0	0.001596
71.36199	2.931141
221.9122	7.580338
372.4623	9.166059
523.0125	8.153888
673.5626	6.819955
824.1128	4.300009
956.3735	-1.82092
974.6629	-2.63212
1125.213	-8.17863
1275.763	-10.5102
1426.313	-9.92998
1576.864	-5.76075
1727.414	3.446591
1877.964	14.95009
2028.514	21.44881
2179.064	21.63149
2329.614	19.66548
2368.525	18.882
2480.164	16.62491
2630.715	13.1011

2781.265	9.471842
2931.815	6.018113
3082.365	2.997144
3232.915	0.547636
3383.465	-1.42884
3534.016	-3.08513
3684.566	-4.48062
3780.677	-5.17803
3835.116	-5.58112
3985.666	-6.31582
4136.216	-6.6833
4286.766	-6.84509
4437.317	-6.67895
4587.867	-5.53305
4738.417	-2.28173
4888.967	4.392655
5039.517	14.54651
5190.067	27.05386
5192.828	27.09844
5340.617	28.0819
5491.168	16.73123
5641.718	9.20074
5792.268	8.750379
5942.818	12.5819
6093.368	15.72846
6243.918	10.69907
6394.469	-8.03521
6545.019	-31.4851
6604.98	-40.71
6695.569	-54.817

6846.119	-73.4845
6996.669	-85.3924
7147.219	-92.2029
7297.769	-95.3874
7448.32	-96.4005
7598.87	-96.6644
7749.42	-98.1281
7899.97	-90.517
8017.132	-84.452
8050.52	-82.7331
8201.07	-76.0439
8351.621	-69.1249
8502.171	-61.2355
8652.721	-58.7051
8803.271	-67.1117
8953.821	-73.0977
9104.371	-75.9691
9254.921	-77.8493
9405.472	-77.0689
9429.283	-76.656
9556.022	-74.2929
9706.572	-70.6044
9857.122	-66.7486
10007.67	-63.1835
10158.22	-60.3449
10308.77	-59.0021
10459.32	-59.8543
10609.87	-62.4532
10760.42	-66.0369
10841.43	-68.2033

10910.97	-70.0697
11061.52	-74.1005
11212.07	-77.6384
11362.62	-79.9786
11513.17	-80.7027
11663.72	-80.3331
11814.27	-79.1305
11964.82	-74.6185
12115.37	-68.1766
12253.59	-61.7693
12265.92	-61.1851
12416.47	-54.2275
12567.02	-47.869
12717.58	-43.0518
12868.13	-43.7118
13018.68	-46.8669
13169.23	-50.5741
13319.78	-53.8676
13470.33	-52.4265
13620.88	-41.8697
13665.74	-38.0792
13771.43	-29.1329
13921.98	-15.9267
14072.53	-2.56223
14223.08	10.55495
14373.63	22.17696
14524.18	22.33612
14674.73	7.856428
14754.56	0.000544